KUOPION YLIOPISTON JULKAISUJA C. LUONNONTIETEET JA YMPÄRISTÖTIETEET 143
KUOPIO UNIVERSITY PUBLICATIONS C. NATURAL AND ENVIRONMENTAL SCIENCES 143

MIIKA NIEMINEN

Quantitative Magnetic Resonance Imaging of Articular Cartilage

Structural, Compositional and Functional Characterization of Normal, Degraded and Engineered Tissue

Doctoral dissertation

To be presented by permission of the Faculty of Natural and Environmental Sciences of the University of Kuopio for public examination in Auditorium L23, Snellmania building, University of Kuopio, on Monday 16th September 2002, at 12 noon

Department of Anatomy
University of Kuopio

KUOPION YLIOPISTO
KUOPIO 2002

Distributor:
Kuopio University Library
P.O.Box 1627
FIN-70211 KUOPIO
FINLAND
Tel. +358 17 163 430
Fax +358 17 163 410

Series editors:
Professor Lauri Kärenlampi, Ph.D.
Department of Ecology and Environmental Science
University of Kuopio

Professor Jari Kaipio, Ph.D.
Department of Applied Physics
University of Kuopio

Author´s address:
Department of Anatomy
University of Kuopio
P.O.Box 1627
FIN-70211 KUOPIO
FINLAND
Tel. +358 17 163 014
Fax +358 17 163 032
miika.nieminen@uku.fi

Supervisors:
Docent Jukka S. Jurvelin, Ph.D.
Department of Applied Physics
University of Kuopio

Professor Heikki J. Helminen, M.D., Ph.D.
Department of Anatomy
University of Kuopio

Professor Risto A. Kauppinen, M.D., Ph.D.
Department of Biomedical NMR
A.I.Virtanen Institute for Molecular Sciences
University of Kuopio

Reviewers:
Associate Professor Deborah Burstein, Ph.D.
Beth Israel Deaconess Medical Center
Department of Radiology
Harvard Medical School, Boston, MA, U.S.A.

Associate Professor Yang Xia, Ph.D.
Department of Physics, Oakland University
Rochester, MI, U.S.A.

Opponent:
Professor Martha L. Gray, Ph.D.
Harvard-MIT Division of Health Sciences and Technology
Massachusetts Institute of Technology
Cambridge, MA, U.S.A.

ISBN 951-781-241-8
ISSN 1235-0486

Kuopio University Printing Office
Kuopio 2002
Finland

Nieminen, Miika. Quantitative Magnetic Resonance Imaging of Articular Cartilage: Structural, Compositional and Functional Characterization of Normal, Degraded and Engineered Tissue. Kuopio University Publications C. Natural and Environmental Sciences 143. 2002. 79 p.
ISBN 951-781-241-8
ISSN 1235-0486

ABSTRACT

Cartilage-related diseases, such as osteoarthrosis (OA), threaten the wellbeing of the human locomotory system, resulting in considerable economic hardship and a decrease in the quality of life of individuals. Quantitative magnetic resonance imaging (MRI) is potentially the best noninvasive means for the characterization of the structure and composition of articular cartilage. In this study, two quantitative ^{1}H NMR relaxation techniques were investigated *in vitro* at 9.4 Tesla using bovine cartilage, one of the techniques being applied *in vivo* to asymptomatic volunteers and orthopaedic patients at 1.0 Tesla.

The effect of enzymatically induced collagen or proteoglycan (PG) degradation on T_2 relaxation time and compressive stiffness of bovine patellar cartilage was investigated. The relationship between the depthwise varying T_2 relaxation time and collagen network anisotropy, as revealed by polarized light microscopy, was surveyed. Gd-DTPA -enhanced T_1 imaging for PGs was correlated with the normal and enzymatically induced depthwise variation of cartilage PG content, as revealed by digital densitometry. Further, the feasibility of using the aforementioned MRI techniques for mechanical characterization of normal bovine humeral and patellofemoral cartilage was explored. Finally, delayed Gd-DTPA -enhanced T_1 imaging *in vivo* was applied in asymptomatic volunteers, and patients who had undergone autologous chondrocyte transplantation surgery and arthroscopic stiffness measurements.

T_2 relaxation time of superficial cartilage was only altered by the digestion of the collagen network, while both digestion of collagen and PGs reduced Young's modulus, a measure of the compressive stiffness of cartilage. In normal tissue, the spatial variation of T_2 was highly correlated with the organization of the collagen network, as assessed by polarized light microscopy. T_1 relaxation time in the presence of the contrast agent Gd-DTPA and MRI-resolved contrast agent concentration correlated highly with the spatial PG content of normal and PG-depleted tissue, however, some overestimation of deep cartilage PGs was observed. T_2 relaxation time and Gd-DTPA -enhanced T_1 imaging parameters were moderately to highly correlated with Young's modulus, dynamic modulus, aggregate modulus and Poisson's ratio of samples. In asymptomatic volunteers, a depth-dependent increase in T_1 relaxation time after intravenous administration of Gd-DTPA was often revealed, this being attributable to the spatial variation in PG content. The technique revealed a PG replenishment in surgically engineered tissue, however, arthroscopic indentation stiffness measurements were indicative of an immature collagen network in grafts.

In conclusion, the investigated quantitative MRI techniques appear as promising tools for the characterization of the structure, composition and functional properties of articular cartilage *in vitro*. Further work is required to demonstrate their suitability for clinical diagnostics.

National Library of Medicine Classification: QT 34, WN 185, WE 300, QS 532.5.C7
Medical Subject Headings: cartilage, articular; magnetic resonance imaging; biomechanics; microscopy, polarization; microspectrophotometry; collagen; proteoglycans; osteoarthritis / diagnosis; chondrocytes / transplantation

To Susanna, Saara and Siiri

ACKNOWLEDGMENTS

This study was carried out during the years 1998-2002 in the Department of Anatomy, University of Kuopio; Department of Clinical Physiology and Nuclear Medicine, Kuopio University Hospital; Department of Biomedical NMR, A. I. Virtanen Institute for Molecular Sciences, University of Kuopio; Mikkeli Central Hospital; and Central Hospital of Central Finland, Jyväskylä.

I owe my deepest gratitude to my principal supervisor Docent Jukka Jurvelin, Ph.D., whose indefatigable spirit and encouragement have guided me throughout these years. It has been an honor to work under his supervision. His expertise and unconditional devotion to science represent the standard for which I want to strive.

I am indebted to Professor Heikki Helminen, M.D., Ph.D., for his fatherly supervision, inspiration and wisdom that he has shared. I am very thankful for the resources of the Department of Anatomy that he has placed at my disposal. I am grateful to Professor Risto Kauppinen, M.D., Ph.D., for his guidance and support, and for providing the NMR facilities for the *in vitro* studies.

I want to express my sincere thanks to the official pre-examiners Associate Professor Deborah Burstein, Ph.D., and Associate Professor Yang Xia, Ph.D., for their constructive criticism and advice that served to improve this thesis. I am grateful to Ewen MacDonald, Ph.D., for linguistic revision.

Working in a multi-laboratory environment has been a highly rewarding experience both professionally as well as in leisure-time activities. With warmth, I remember every "manager" of our Biophysics of Bone and Cartilage Group, the senior and junior researchers and staff members in the Department of Anatomy, the NMR group in the A. I. Virtanen Institute, and the collaborators of the *in vivo* studies. My special thanks go to Juha Töyräs, Ph.D., and Jarno Rieppo, B.M., for the companionship and invaluable cooperation since the very onset of our scientific struggles. I want to thank Johanna Närväinen (née Silvennoinen), M.Sc., and Juhana Hakumäki, M.D., Ph.D., for their dedication, and the expertise in MRI that they willingly shared. I am grateful to Mika Hyttinen, M.D., for his contribution to the quantitative microscopy and Mikko Laasanen, B.Sc., for biomechanical testing. For fruitful *in vivo* collaboration I want to thank Jari Heikkinen, Ph.D., Heikki Hermunen, M.D., Ilkka Kiviranta, M.D., Ph.D., Anna Vasara, M.D., Jarmo Toivanen, Ph.D., and Eeva Elomaa, M.D.. Mrs. Eija Rahunen and Mr. Kari Kotikumpu deserve credit for skillful histological sample preparation, and Kari Mauranen, M.Sc., for statistical advice.

I want to thank Atria Lihakunta Oyj, Kuopio, and their personnel for providing material for the *in vitro* part of this study.

I am eternally grateful to my parents Marja-Leena and Risto Nieminen for their encouragement and support, and for passing on their faith, creativity and courage. The company and support of my brother Heikki and sister Anni has been crucial

and invigorating. I am thankful to all my friends, relatives and band-mates for their support and attempts to keep my thoughts away from work.

Finally, my utmost and dearest thanks go to my beloved wife Susanna for her continuous support, understanding and love, and to our ever-so-lovely daughters Saara and Siiri. Their presence has made my efforts possible and meaningful.

This study was financially supported by the Finnish Graduate School in Skeletal Diseases, the Ministry of Education in Finland, Kuopio University Hospital (EVO grant 5103), the National Technology Agency (TEKES), the Instrumentarium Science Foundation, the Research Foundation of Orion Corporation, the Kuopio University Foundation and the Sigrid Juselius Foundation, which I acknowledge with gratitude.

Kuopio, August 2002

Miika Nieminen

ABBREVIATIONS AND NOTATIONS

ACT	autologous chondrocyte transplantation
ADC	apparent diffusion coefficient
DD	digital densitometry
dGEMRIC	delayed Gadolinium Enhanced MRI of Cartilage
GAG	glycosaminoglycan
Gd-DTPA	gadolinium diethylene triamine pentaacetic acid
[Gd-DTPA]	molar concentration of Gd-DTPA
G_{ss}, G_{pe}, G_{fe}	slice select, phase encoding and frequency encoding gradients
ECM	extracellular matrix
FCD	fixed charge density
FEM	finite element modeling
FID	free induction decay
FOV	field of view
MT	magnetization transfer
MRI	magnetic resonance imaging
NMR	nuclear magnetic resonance
OA	osteoarthrosis
PBS	phosphate buffered saline
PG	proteoglycan
PLM	polarized light microscopy
r.f.	radio frequency
sd	standard deviation
SI	signal intensity

a	activity of ion
a_c	contact radius of indenter
a_F	optical constant
a_λ	wavelength-dependent absorptivity coefficient
A	absorbance
b_F	optical constant
$\boldsymbol{B}$	magnetic field strength
$\boldsymbol{B}_0$	static magnetic field strength
BF	optical birefringence of polarized light
C	molar concentration
E_s	Young's modulus
E_d	dynamic modulus
E_1	storage modulus
E_2	loss modulus
$\hbar$	Dirac's constant

H_a	aggregate modulus
$\boldsymbol{i}$,$\boldsymbol{j}$,$\boldsymbol{k}$	vectors pointing at x, y and z directions
l	section thickness
$\boldsymbol{M}$	angular momentum
m	molality
I	intensity
I_0	initial intensity
k	Boltzmann constant
OD	optical density
p	statistical significance
r	Pearson correlation coefficient
r_{dd}	dipole separation
R	relaxivity
R_g	universal gas constant
SD	spin density
t	time
T	absolute temperature
T_l	transmittance
TE	echo time
TI	inversion time
TR	repetition time
T_1	spin-lattice relaxation time
$T_{1\mathrm{Gd}}$	spin-lattice relaxation time in presence of Gd-DTPA
$T_{1\rho}$	spin-lattice relaxation time in the rotating frame
T_2	spin-spin relaxation time
z	valency of ion
α	rotation angle of polarization plane
γ	gyromagnetic ratio
Γ	activity coefficient
ϵ	strain
θ	angle between the vector joining two dipoles and $\boldsymbol{B}_0$
λ	wavelength
ν	Poisson's ratio
ω	angular frequency
ω_0	angular Larmor frequency
π	constant
Π	osmotic pressure
σ	stress
σ_d	dynamic stress
τ_c	correlation time
ϕ	osmotic coefficient of ion

LIST OF ORIGINAL PUBLICATIONS

This thesis is based on the following original articles referred to by their Roman numerals:

I Nieminen MT, Töyräs J, Rieppo J, Hakumäki JM, Silvennoinen J, Helminen HJ, Jurvelin JS. Quantitative MR microscopy of enzymatically degraded articular cartilage. Magnetic Resonance in Medicine 43: 676-681, 2000.

II Nieminen MT, Rieppo J, Töyräs J, Hakumäki JM, Silvennoinen J, Hyttinen MM, Helminen HJ, Jurvelin JS. T_2 relaxation reveals spatial collagen architecture in articular cartilage: a comparative quantitative MRI and polarized light microscopic study. Magnetic Resonance in Medicine 46: 487-493, 2001.

III Nieminen MT, Rieppo J, Silvennoinen J, Töyräs J, Hakumäki JM, Hyttinen MM, Helminen HJ, Jurvelin JS. Spatial assessment of articular cartilage proteoglycans with Gd-DTPA -enhanced T_1 imaging. Magnetic Resonance in Medicine, in press.

IV Nieminen MT, Töyräs J, Laasanen MS, Silvennoinen J, Helminen HJ, Jurvelin JS. Estimation of biomechanical properties of articular cartilage using quantitative magnetic resonance imaging. Manuscript, submitted for publication.

The thesis also contains previously unpublished data.

Chapter I
Introduction

Osteoarthrosis (OA), a disease of increasing prevalence and impairment, affects the wellbeing of countless individuals on a global scale and leads to a huge economic burden on the society. In United States, different forms of arthritis have resulted in costs of 64.8 billion dollars in 1992 [166]. The total costs related to musculoskeletal conditions were 149.4 billion dollars, of which approximately half was due to direct medical expenses and the rest due to lost wages.

The first sign of OA is the degeneration of the extracellular matrix of articular cartilage. This leads to an impairment in the mechanical properties of cartilage tissue, critical to normal joint function. Erosion of cartilage tissue begins and, when it has sufficiently progressed, the only therapy is total joint replacement. Conventional clinical modalities, such as X-ray imaging of joint space narrowing and invasive arthroscopy, are frequently too insensitive to detect the early stages of the disease process. Thus, there is a need for quantitative techniques that would enable the evaluation of the structural and compositional, or even the mechanical, integrity of the tissue. These techniques would also serve in predicting the outcome of rapidly developing tissue engineering approaches for cartilage repair.

Magnetic resonance imaging (MRI) has proven to be essential in the diagnostics of musculoskeletal diseases [106]. Increase in magnetic field strengths and other advances in imaging technology enable the effective noninvasive evaluation of subtle, highly specialized tissues such as articular cartilage. Particularly, ^{1}H nuclear magnetic resonance (NMR) relaxation properties of tissue can provide previously unattainable information on the macromolecular phase of tissue that interacts with MRI-visible water protons. Thus, quantitative MRI holds great potential for future diagnostics of degenerative joint diseases.

In this study, a high magnetic field approach was used to develop, validate and apply two quantitative MRI techniques for the evaluation of the structure, composition and mechanical characteristics of articular cartilage. One of the techniques was further applied *in vivo*. Quantitative microscopic assessment of the tissue ul-

trastructure and/or biomechanical measurements provided a selection of sensitive reference techniques for the characterization of normal, enzymatically degraded and engineered cartilage tissue.

Chapter II

Structure of articular cartilage

2.1 Cartilage constituents

Articular cartilage is a highly specialized, avascular and aneural translucent tissue that forms smooth gliding surfaces at the ends of articulating bones. Cartilage has a demanding mechanical task to resist loads that are transmitted through joints, and it provides almost frictionless surfaces to allow unhampered locomotion. Cartilage consists of three main phases: (*i*) the interstitial water that comprises 60-80% of the wet weight, (*ii*) chondrocytes that occupy about 1% of the tissue wet weight, and (*iii*) the extracellular matrix (ECM), *i.e.* the collagen network and proteoglycans (PGs), that account for the remaining 20-30% of weight [107]. The cartilage thickness, typically 2-5mm for human, and mechanical properties vary between species and different joints [139, 11].

2.1.1 Collagen network

Fibril-forming collagens, mainly of type II collagen, form a highly organized, an isotropic three-dimensional fibrous network in articular cartilage. Collagen is the major constituent of cartilage, accounting for the largest portion of organic material in the tissue, 15-22% of tissue wet weight [117]. The basic element in collagen is a coiled structure composed of three polypeptide chains, each with an elastic modulus of about 270MPa [148], forming a right-handed triple helix of 1.5nm in diameter [154]. These architectural building blocks further form fibrils together with other matrix macromolecules [44], with diameters ranging from 20 to 200nm [117]. The relative portion of collagen of tissue dry weight decreases from superficial to deep cartilage [153].

Using polarized light microscopy (PLM), Benninghoff demonstrated the varying arrangement of collagen fibrils at different depths of cartilage (Fig. 2.1) [19]. According to this model, cartilage can be divided depthwise to zones in terms of its collagen fibril arrangement:

1. the tangential zone (superficial zone): collagen fibrils are arranged in parallel to the articular surface and begin to arcade towards zone 2. The zone shows a high PLM signal. This accounts for approximately 5-15% of the total cartilage thickness in human;

2. the transitional zone (intermediate zone): superficial fibrils have turned to form a randomly organized meshwork of fibrils in this zone. Isotropy results in low or null PLM signal. Approximately 1-15% of the thickness;

3. radial zone (deep zone): fibrils of the transitional zone become radially arranged and are anchored to the calcified cartilage at the cartilage-bone-interface (often a tidemark is seen at this interface). The PLM signal is high in this zone. The zone accounts for about 70-90% of the cartilage thickness.

This characterization provides a framework to describe the cartilage structure, for example, by measuring thicknesses or quantitative optical parameters, such as birefringence of polarized light, in different tissue zones [8, 7]. Recent studies, however, have demonstrated that the collagen network, in fact, may be more complicated [61, 164]. For example, the fibrils were reported to be differently organized in the weight-bearing and non-weight-bearing regions of the joints [45, 57].

2.1.2 Proteoglycans

PGs are the other major macromolecular constituent of cartilage in addition to collagen, and account for 4-7% of the tissue wet weight [117]. PGs consist of a core protein, which has covalently bonded glycosaminoglycan (GAG) chains attached to it. Chondroitin- and keratan-sulfated GAGs are the most abundant GAGs found in cartilage. PG monomers combine to form large aggregates [118, 65]. The sulfate and carboxyl groups of chondroitin and keratan sulfate are negatively charged, giving rise to a high fixed charge density (FCD) of the tissue. Together with the collagen network, PGs account for the complex electromechanical and physicochemical interactions in cartilage [63, 46, 47].

If a sample of cartilage is placed in an electrolyte solution, the fixed charge in cartilage attracts external positive ions from the solution to satisfy the electroneutrality condition of the ion concentrations in cartilage

$$z_{\text{cation}} C_{\text{cation}} = z_{\text{anion}} C_{\text{anion}} + C_{\text{immobile anion}}, \tag{2.1}$$

where C is the molar concentration of ions and z is their valency. The distribution of small ionic solutes is considered to obey the Donnan equilibrium equation [100]

$$\left(\frac{a'_{\text{cation}}}{a_{\text{cation}}}\right)^{z_{\text{cation}}} = \left(\frac{a_{\text{anion}}}{a'_{\text{anion}}}\right)^{z_{\text{anion}}}, \tag{2.2}$$

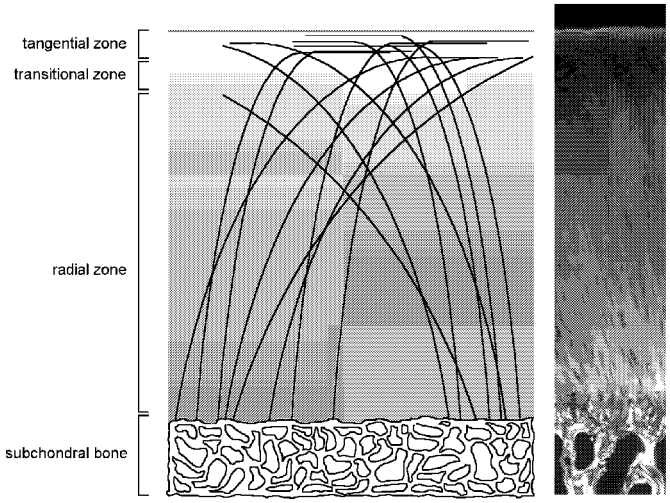

Figure 2.1: Macromolecular structure of articular cartilage (left): the three-dimensional collagen network (black lines) and the depthwise PG concentration gradient (tone darkens with increasing concentration). Polarized light microscopic image (right) of human cartilage is shown (2.5× magnification).

where a and a' refer to the activities of ions in cartilage and solution, respectively ($a = \Gamma m$, Γ = activity coefficient, m = molality). The Donnan effect will result in an unequal distribution of diffusible ions between the tissue and solution. Since more molecules (mobile ions and macromolecules) are present in cartilage, the resulting osmotic imbalance is counteracted by the in-flow of water. The osmotic pressure is given by the difference of pressures between the two compartments

$$\Delta\Pi = \Pi - \Pi'. \tag{2.3}$$

In unloaded tissue, this pressure is counterbalanced by tensile forces of the elastic collagen network. Since osmotic pressure is dependent on the number of active particles, not their size, the ionic Donnan contribution is believed to be mainly responsible for $\Delta\Pi$ [100]. For the Donnan contribution of cations and anions i

$$\Pi = R_g T \sum_i \phi_i m_i \tag{2.4}$$

$$\Pi' = R_g T \sum_i \phi_i' m_i', \tag{2.5}$$

where R_g is the universal gas constant, T is absolute temperature, m is the molal concentration of ions and ϕ is the osmotic coefficient of cations or anions in different compartments.

PGs are nonhomogeneously distributed throughout cartilage. In healthy tissue, the PG concentration is lowest at the articular surface and increases when one moves towards deeper parts of the tissue. Often a plateau is observed in the PG concentration of deep cartilage [101, 81].

2.1.3 Interstitial water

The space surrounding macromolecules and chondrocytes is filled with water, having electrolytes dissolved in it. A small amount of water is contained in chondrocytes. About 30% of water is in the intrafibrillar space within collagen fibrils, while the remainder exists in the solution formed by water and PGs [118]. The major fraction of interstitial water is free and exchangeable [103]. A distinct water-rich layer can be found surrounding the collagen fibrils, possibly related to a shield produced by type IX collagen and small PGs decorating the surface of type II collagen [147].

The water content of the tissue is governed by (*i*) the concentration of PGs and the resulting swelling pressure, (*ii*) organization of the collagen network and (*iii*) the strength and stiffness of the collagen network that resists PG swelling [2, 105, 104]. Thus, the anisotropic structure and composition of the ECM results in an nonhomogeneous distribution of water. The water content is highest in the superficial tissue and decreases towards the deep tissue [90, 22].

2.1.4 Chondrocytes

Chondrocytes are specialized cells that manufacture and maintain the ECM. Cartilage is relatively acellular. Cells occupy 1-10% of the tissue volume, yet the relatively few chondrocytes are capable of producing the fibril-reinforced gel structure of collagen and PGs. This function persists through adult life [146, 119].

In human, the number and shape of chondrocytes change with depth of cartilage. The cells are most numerous in the superficial zone, where they are small and flattened in shape. In intermediate tissue, chondrocytes are moderate in size with an oval or rounded shape. The deep tissue is occupied by large rounded cells arranged in vertical columns [33, 146].

2.1.5 Interaction between constituents

The collagen network and PGs in articular cartilage are functionally interdependent. Molecular interactions occur via collagen-collagen, PG-collagen and PG-PG interactions, that are important for the functional integrity of the tissue [23, 118]. Covalent collagen-collagen cross-linking is essential in providing a strong and stiff collagen network [117]. The physical interaction between collagen and PGs can

arise from either (*i*) electrostatic forces, in which negative groups of GAGs interact with positively charged groups of collagen or (*ii*) due to the strong frictional interaction between PGs and the collagen network when the swelling pressure of PGs is restricted by the collagen framework [117, 134]. The PG-PG interaction within cartilage arises from the repulsive forces between negatively charged GAGs [117]. The size of PGs and their ability to form large aggregates have an important role in retaining the molecules in the tissue [126]. Finally, the interaction between matrix macromolecules and the solvent accounts for swelling by the affinity of the ECM to imbibe water [42].

2.2 Osteoarthrosis

OA is a destructive joint disease that is one of the most common causes of impairment of middle-aged and elderly people. It is characterized by a progressive deterioration and localized erosion of cartilage, remodeling of subchondral bone and formation of osteophytes, though the disease usually involves all tissues that form the synovial joint [25]. The disruption of the cartilage ultrastructure dramatically impairs the mechanical characteristics of the tissue [6], leading to an imbalance between the mechanical demands and joint loading. In spite of the highly developed structure with remarkable mechanical characteristics of healthy tissue, cartilage lacks the capacity to adequately repair structural damage, especially that of the collagen network [25].

The first signs of cartilage degeneration involve PG loss, disruption of the collagen network, an increase in the water content and remodeling of subchondral bone [22, 14, 99, 129]. In the second stage, chondrocytes respond to alterations by increasing the synthesis and degradation of the matrix molecules, aiming at restoring the normal tissue structure and composition. Finally, the failure of the chondrocytic response leads to a loss of cartilage, probably related to mechanical damage of the tissue [25].

A major problem in the diagnosis of cartilage-related diseases arises from the fact that the early stages of disease are often asymptomatic due to the anervous structure of the tissue. When symptoms do occur, intervention is often necessary. Surgical repair techniques have been developed in the past decades to restore the articular cartilage in joints. These methods include osteotomy, débridement and penetration of the subchondral plate, allogenous or autogenous grafts and autologous chondrocyte transplantation [121, 25]. There is a clear need for quantitative techniques to detect cartilage degeneration and monitor the outcome of rapidly advanced cartilage engineering techniques. Conventional diagnostic modalities, such as X-ray imaging of joint space narrowing and invasive arthroscopic examination, are often too insensitive to reveal the early stages of the disease process before macroscopic changes in tissue start to appear. The advanced use and development of both qualitative

and quantitative MRI techniques have brought a considerable improvement in this respect [26, 106, 4].

Chapter III

Quantitative microscopy of articular cartilage

3.1 Polarized light microscopy of collagen network

Anisotropically organized small tissue structures that generate larger macrostructures, such as collagen in articular cartilage, exhibit the optical property of double refraction or birefringence (BF), *i.e.* the capability to rotate the plane of polarized light [18]. This is defined by

$$BF = \frac{\alpha\lambda}{\pi l}, \tag{3.1}$$

where α is the rotation angle of the polarization plane, λ is the wavelength of monochromatic light, π is the mathematical constant, and l is the optical path length. If an unstained microscopic section is placed in between two perpendicularly crossed polarizers under monochromatic light, the optical activity of the sample gives rise to an image. The light that is transmitted through the system is dependent on the organization, *i.e.* anisotropy, and the orientation of the collagenous structures. The intensity of emerging light I can be related to the angle of rotation in the form of the Fresnel equation

$$I = a_F + b_F I_0 \sin^2 \alpha, \qquad 0 \leq \alpha \leq \pi/2, \tag{3.2}$$

where I_0 is the intensity of light after the first polarizer, and a_F and b_F are optical constants characteristic to the microscope system. After solving for α in Eq. (3.2), Eq. (3.1) yields

$$BF = \frac{\lambda}{\pi l} \arcsin \sqrt{\frac{I - a_F}{b_F I_0}}. \tag{3.3}$$

Principally, quantitative PLM techniques allow the separation of the contribution of organization and orientation of the collagen network. The system of crossed polarizers, with a $\lambda/4$ compensator in between, can be adjusted to visualize the tangential and radial collagen network with respect to the articular surface. The sensitivity

of detection, however, is dependent on the angle of the fibrils themselves. When approaching the oblique, 45° direction, detection sensitivity gradually decreases and finally becomes zero. Further, a parallel 45° rotation of the polarizers makes the system sensitive to the fibrils at 45° orientation, and it is now insensitive to the tangential and radial directions. With these adjustments, combining two images by applying the Boolean maximum function ($\texttt{max}(x, y) = x$, when $x > y$) for corresponding pixels, an image is produced that reflects exclusively the local isotropy, *i.e.* the local organization of the collagen network, while the contribution of the fibril orientation is minimized. Low or missing local BF refers to tissue structures with a low degree of organization, typically observed in the intermediate zone, whereas high values from anisotropic structures are recorded in both the superficial and deep tissue [19, 18].

3.2 Digital densitometry of proteoglycans

Charged, orthochromatic dyes have successfully been used for microspectrophotometric semiquantitative estimation of PGs in cartilage [80]. Cationic dyes, such as Safranin-O or Alcian blue, attach to the charged groups of GAGs at optimal pH conditions. Consequently, the absorbance (A) of electromagnetic radiation by a specimen, also known as the optical density (OD), is linearly related to the amount of fixed charge [81, 80]. The Beer-Lambert law defines the linear relationship between the absorbance and the concentration of a dye (C)

$$A = a_\lambda C l, \tag{3.4}$$

where a_λ is the wavelength-dependent absorptivity coefficient and l is the pathlength. The absorbance of a microscopic section can be calculated from the ratio of transmitted and initial intensity of light, *i.e.* transmittance T_l:

$$A = -\log(T_l) = -\log\left(\frac{I}{I_0}\right). \tag{3.5}$$

Since absorption is a linear, semiquantitative measure for PGs, calibration with an appropriate filter set will allow one to relate the transmission of light to a specific OD value, depicting the concentration of PGs within microscopic sections of articular cartilage [81, 80].

Chapter IV

Mechanical properties of articular cartilage

4.1 Measurement geometry

The mechanical characterization of articular cartilage is essential for one to understand its function and competence to fulfill the demanding biomechanical task. Mechanical properties can be determined using load-deformation experiments, that disturb the balance between the swelling pressure of PGs and the restrictive forces attributable to the collagen network.

Loading geometries are classified according to the indenter and sample confinement (Fig. 4.1). *Indentation* is a traditional *in situ* measurement geometry, in which intact or isolated cartilage is pressed with a perpendicularly-aligned rigid impervious or permeable indenter that is typically plane- or spherical-ended. The indenter radius should be small enough as compared to the diameter of the sample, otherwise sample boundaries may affect the material characterization [143]. In *unconfined compression*, the sample detached from the subchondral bone, is deformed between two smooth impervious metallic platens, allowing fluid flow in lateral direction. In *confined compression* the sample is inserted in a confining chamber to prevent lateral expansion, and loaded with a permeable piston to allow axial out/in-flow of fluid from the sample. Three loading schemes are typically applied, *i.e.* the *stress-relaxation*, *creep*, and *dynamic* loading. In the first, a constant deformation is applied and the relaxation of the reaction force is measured as a function of time. The creep test involves a constant stress while the displacement of the tissue is recorded. In dynamic loading, several sinusoidal cycles are applied at a certain frequency and stress or strain amplitude.

4.2 Mechanical parameters

Various models have been developed to characterize the loading response of articular cartilage. Most of these consider cartilage to be homogenous and isotropic material

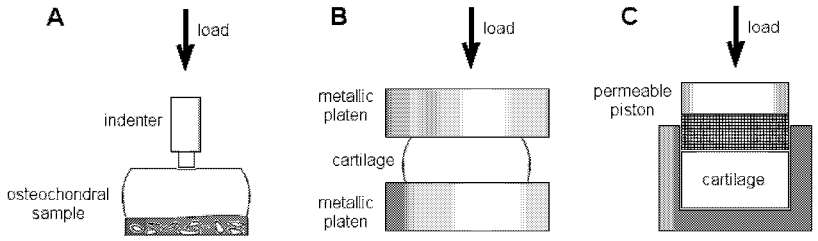

Figure 4.1: Different loading geometries for mechanical measurements of cartilage: (A) indentation, (B) unconfined compression, and (C) confined compression geometries.

for the sake of simplicity. These include the *elastic* model that treats the tissue as an elastic single phasic solid [67], the *viscoelastic* model [123], the *biphasic* model [116] and the *triphasic* model [85]. Recently developed models, such as the *transversely isotropic biphasic* [32] and *fibril reinforced* models [142, 93, 83], attempt to account for the more complicated cartilage structure.

For an elastic material that is compressed in unconfined geometry (Fig. 4.1B), Young's modulus at equilibrium is determined as the ratio of axial stress (σ) and strain (ϵ):

$$E_s = \frac{\sigma}{\epsilon}. \tag{4.1}$$

For indentation, Hayes *et al.* (1972) originally derived the solution [67]

$$E_s = \frac{\sigma}{\epsilon} \frac{\pi a_c (1 - \nu^2)}{2h\kappa}, \tag{4.2}$$

where a_c is the contact radius of a plane-ended indenter, ν is Poisson's ratio, h is cartilage thickness and $\kappa(\frac{a_c}{h}, \nu)$ is a theoretical scale factor that accounts for the finite and variable cartilage thickness [67]. To eliminate the time-dependent poroviscoelastic behavior of cartilage, E_s is typically measured from the equilibrium response.

Dynamic modulus of cartilage is measured to observe the response of the tissue on a cyclic deformation at a particular frequency [66, 88]. The dynamic modulus (E_d) for a viscoelastic material is complex in nature:

$$E_d = E_1 + iE_2, \tag{4.3}$$

where E_1 is the *storage modulus*, proportional to the elastically stored energy, and E_2 is the *loss modulus*, describing the viscous energy dissipated in the loading

process. Typically the complement of E_d is presented and becomes reduced to the form

$$|E_d| = \sqrt{{E_1}^2 + {E_2}^2} = \frac{\sigma_d}{\epsilon}, \tag{4.4}$$

where σ_d is the dynamic stress exerted on the sample. Due to the instantaneous incompressibility of cartilage, the dynamic modulus for cartilage is typically several times the equilibrium modulus [29].

Poisson's ratio describes the lateral expansion of an axially compressed sample, and is defined as the ratio of lateral and axial strains. It describes the compressibility of material. Typical values for ν of cartilage range between 0 and 0.2 in different human joints [11, 9, 10, 71]. Instantaneously cartilage is virtually incompressible under infinitesimal strain, *i.e.* $\nu \approx 0.5$ [72, 158].

Based on the assumption of material isotropy, the aggregate modulus (H_a), *i.e.* the equilibrium modulus in confined compression, is related via E_s and ν through the relation [72]

$$H_a = \frac{(1-\nu)}{(1+\nu)(1-2\nu)} E_s. \tag{4.5}$$

Values for H_a and E_s typically range between 0.5-1.8MPa in healthy human cartilage, depending on the joint and topographical location [6, 11, 9, 10, 51].

4.3 Structure-function relationships

Physiological joint loading of articular cartilage generates compressive, tensile and shear stresses. The poroviscoelastic response of the tissue arises from the composition, structure and interaction of the ECM constituents, and the flow of interstitial fluid through the permeable matrix. Upon load, the tissue relaxes and rearranges itself to reach equilibrium. Removal of the load leads to a resorption of fluid and the tissue regains its initial configuration.

For cartilage, the interstitial deformation of tissue depends on the depth of tissue and is attributed to the nonhomogeneous and anisotropic structure of the ECM [72]. The rigid collagen structure in the superficial tissue allows less lateral expansion as compared to deeper parts of the tissue where the network is not arranged to resist lateral expansion in an effective manner.

In cartilage, the swelling of PGs is restricted by elastic forces of the collagen network, providing the tissue resilience [109]. During instantaneous load, cartilage shows an elastic deformation with no out-flow of fluid [100]. The collagen network is mainly responsible for controlling this deformation [109, 13]. Finite element modeling (FEM) has revealed the important role of the superficial tissue layer in the indentation geometry [83]. The degradation of the collagen network correlates with the instantaneous deformation [14].

The porous properties of cartilage that are effective after the instantaneous deformation arise primarily from PGs, and act to restrict out-flow of water by governing the permeability of tissue [102, 13]. Tissue permeability and solute diffusivity decrease with compressive load [27, 127, 128], and water content correlates positively with permeability [6]. Compressive equilibrium moduli correlate positively with the GAG content and negatively with the hydration of cartilage [75, 6].

Chapter V

MRI of articular cartilage

5.1 ^{1}H nuclear magnetic resonance

5.1.1 Precession and excitation

Non-interacting proton spins may occupy two different spin states. When experiencing an external static magnetic field $\boldsymbol{B}_0$, the coupling between the proton and the external field results in an uneven distribution of the proton populations at +1/2 (lower) and -1/2 (higher) spin states, given by the Boltzmann law

$$\frac{n_{-1/2}}{n_{+1/2}} = e^{-\Delta E/kT} = e^{-\gamma\hbar B_0/kT}, \tag{5.1}$$

where n represents the number of spins at different states, ΔE is the energy difference between the states, γ is the gyromagnetic ratio, T is the temperature, k is the Boltzmann constant and $\hbar$ is Dirac's constant. The difference between energy states gives rise to the concept of *net magnetization*, by which an ensemble of protons can be treated in a semi-classical manner [30, 35, 64] possessing a macroscopic angular momentum $\boldsymbol{M}$. The external static magnetic field $\boldsymbol{B}_0$ causes a change in angular momentum, given by

$$\frac{d\boldsymbol{M}}{dt} = \gamma \boldsymbol{M} \times \boldsymbol{B}_0. \tag{5.2}$$

The precessional angular frequency ω_0, known as the Larmor-frequency, is directly proportional to the amplitude of the external field

$$\omega_0 = \gamma B_0, \tag{5.3}$$

where $\gamma = 2.675{\times}10^8$ rad s^{-1}T^{-1} for ^{1}H nuclei. The application of an additional transverse on-resonance field, *i.e.* a radio frequency (r.f.) pulse at Larmor frequency

$$\boldsymbol{B}_1(t) = B_1 \cos\omega_0 t\boldsymbol{i} - B_1 \sin\omega_0 t\boldsymbol{j} \tag{5.4}$$

results in a time-dependent behaviour of $\boldsymbol{M}$ in a three-dimensional coordinate system. Equations (5.2) and (5.4) yield

$$\frac{dM_x}{dt} = \gamma \left(M_y B_0 + M_z B_1 \sin \omega_0 t\right) \tag{5.5}$$

$$\frac{dM_y}{dt} = \gamma \left(M_z B_1 \cos \omega_0 t - M_x B_0\right) \tag{5.6}$$

$$\frac{dM_z}{dt} = -\gamma \left(M_x B_1 \sin \omega_0 t + M_y B_1 \cos \omega_0 t\right). \tag{5.7}$$

5.1.2 Relaxation

The momentary resonant r.f. pulse disturbs the thermal equilibrium of the spin system. Following the excitation, the time-dependent evolution of net magnetization is given by the Bloch equations, derived from (5.5)-(5.7), by supplementing with appropriate decay terms. The equations of motion are [35, 64]

$$\frac{dM_x}{dt} = \omega_0 M_y - \frac{M_x}{T_2} \tag{5.8}$$

$$\frac{dM_y}{dt} = -\omega_0 M_x - \frac{M_y}{T_2} \tag{5.9}$$

$$\frac{dM_z}{dt} = \frac{M_0 - M_z}{T_1} \tag{5.10}$$

with relaxation time constants T_1 and T_2. The cylinder symmetric equations (5.8) and (5.9) yield

$$M_x(t) = e^{-t/T_2}(M_x(0)\cos \omega t + M_y(0)\sin \omega t) \tag{5.11}$$

$$M_y(t) = e^{-t/T_2}(M_y(0)\cos \omega t - M_x(0)\sin \omega t). \tag{5.12}$$

Solving for M_z in (5.10) gives

$$M_z(t) = M_z(0)e^{-t/T_1} + M_0(1 - e^{-t/T_1}). \tag{5.13}$$

Dipole-dipole coupling is the main source of NMR relaxation in solution or tissue when ^{1}H protons are the nuclei of interest. Also known as the longitudinal or spin-lattice relaxation, the time constant T_1 in (5.10) characterizes the rate of energy transfer between a spin and its surroundings, *i.e.* the lattice. Energy exchange will occur until spins and the lattice are in thermal equilibrium (see (5.1)). Similar to the effect of an external resonant field, nuclear spins are affected by nearby

time-dependent magnetic fields that arise from rotational molecular motions, chemical exchange and spin diffusion. Also, paramagnetic species or electric quadrupole interaction of non-1/2-spin nuclei may provide powerful relaxation mechanisms.

The time component of field fluctuations is characterized by the *correlation time* τ_c. Correlation times vary from $\sim 10^{-12}$s for bulk water up to $\sim 10^{-3}$s for tightly bound hydration water [24, 52, 82, 92].

The magnetic field of a spin exerted on another depends on both its separation and relative orientation in the magnetic field (Fig. 5.1). For the transverse component

$$B_{xy} = \frac{3\gamma}{2\hbar r_{dd}^3} \sin\theta \cos\theta. \tag{5.14}$$

For the relaxation rate

$$\frac{1}{T_1} \propto B_{xy}^2 \frac{\tau_c}{1+\omega_0^2\tau_c^2}. \tag{5.15}$$

Clearly, the relaxation is most efficient when $\tau_c = 1/\omega_0$.

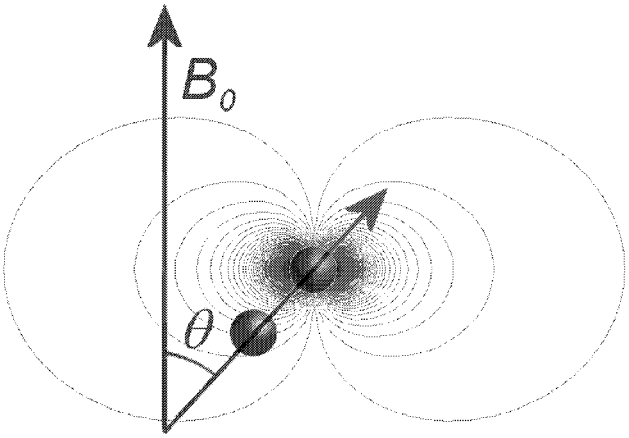

Figure 5.1: The angle-dependent dipolar effect exerted by a proton magnetic field on another proton in a static magnetic field B_0. θ represents the angle between the vector joining the dipoles and $\boldsymbol{B}_0$.

T_2 relaxation, also known as transverse or spin-spin relaxation, depicts relaxation processess that involve the interaction of neighboring spins without any exchange of energy with the lattice. Molecular motions with $\omega \leq \omega_0$ will disturb the phase coherence of spins and lead to the decay of magnetization in the xy-plane, as described

by the time constant T_2. For the transverse relaxation rate

$$\frac{1}{T_2} \propto B_z^2 \tau_c. \tag{5.16}$$

Thus, transverse relaxation is more efficient at slower correlation times.

A mechanism of B_z variation can be the orientation-dependent dipolar field of a proton on another given by

$$B_z = \frac{\gamma}{2\hbar r_{dd}^3} \left(3\cos^2\theta - 1\right). \tag{5.17}$$

With isotropic molecular motion, as in non-viscous liquids, this angular dependence of dipole-dipole interaction averages to zero, and known as *motional narrowing*. However, in substances where the rotational motion is restricted and anisotropic, or even fixed as in solids, the effect described by (5.17) may induce a significant source of magnetic field inhomogeneity and thus contribute to $\Delta\omega$ and consequently to T_2, as seen in (5.16). It is readily seen from (5.17) that the "static" dipolar effects arising from the anisotropy are minimized when $\theta \approx 54.7°$, known as the *magic angle*. Andrew *et al.* (1959) were the first to show that the resonance linewidth in solids, usually very broad, could be narrowed down by a specimen rotation at this critical angle [5]. For tissues, such orientational dependence of T_2 contrast has been reported for tendons [20], cartilage [132] and blood vessel capillaries [122]. These premises of structural anisotropy-related NMR contrast can be expanded also to proton double-quantum filtered MRI studies [120].

5.1.3 Physiological basis of relaxation

As described above, magnetic dipole-dipole coupling is the main source of NMR relaxation in solution or tissue when hydrogen protons are the nuclei of interest. Rapid molecular motions comparable to the Larmor frequency provide a source of dynamic dipolar interaction by spin exchange, and contribute to both T_1 and T_2 relaxation. Slower motions of the water-macromolecule system, on the other hand, result in a "static" component of magnetic coupling. This will contribute only to T_2 relaxation by a dephasing effect, a result of differences in resonant frequencies. Since slow macromolecular motions are always present in biological tissues, $T_2 << T_1$. Thus, T_2 is sensitive to the molecular mobility and the size of the surrounding molecules, though the processes are also temperature and pH dependent [24]. The relaxation rates are frequency dependent and therefore the measured relaxation times may vary with the field strength B_0 used.

The majority of water in tissue is usually free, while structured and bound pools, *i.e.* hydration water, represent the other abundant proton populations [52]. Although water molecules in tissue are estimated to spend less than 2% of their time

in contact with the macromolecules, the NMR relaxation properties of water are significantly affected by these interactions [82]. In particular, magnetic interactions between protons are sensitive to the slowing of the rotational motion of water molecules during these contacts and successive interactions lead to relaxation. Exchange processes between bound and bulk water pools transfer the relaxation effects to the MRI-visible compartment that has relatively high correlation times as compared to the macromolecules and bound water. The relaxation response of water interacting with macromolecules has contributions from (*i*) *proton exchange* between water and protein ionizable groups, (*ii*) *water molecule exchange* with specific protein sites, and (*iii*) *transient collisions* between water and proteins at the hydration layer [24]. For hyaline cartilage, Fullerton (1992) presented NMR titration (dehydration) plots that suggested the presence of only bulk and bound water pools [52]. Recently, a four spin reservoir model for articular cartilage was suggested, involving magnetization exchange between collagen-bulk water, proteoglycan-collagen and collagen fibrillar water-collagen subsystems [86]. In the model, the collagen-bulk water was the largest coupling subsystem and thus exploited in MRI. Biological samples possess a distribution of correlation times due to the several interaction mechanisms. Biochemical changes, *e.g.* in disease process, may alter this distribution and this may be observed by measuring relaxation times in tissue.

5.1.4 Measurement of T_1 and T_2

As described in Section 5.1.1, the B_1 field is applied to saturate the spin system. This is immediately followed by the recovery of magnetization characterized by the time constant T_1. A 90°-pulse turns the spin magnetization into the transverse plane. If another pulse is applied amidst the relaxation process after a time TR (repetition time), the signal prior to re-excitation will have a certain amount of T_1-weighting. Consecutive measurements with varying TR will yield a magnetization profile which can be used to solve for the time constant T_1 in (5.13). The same effect can be achieved by using the spin-echo sequence, introduced later, with varying TR. An alternative techique is to apply a 180°-pulse that causes the inversion of magnetization. After a time TI (inversion time) a 90°-pulse is applied to provide a snapshot of the magnetization. Depending on the scheme selected, (5.13) will have a different form; for *saturation recovery*

$$M_z(TR) = M_0(1 - Ae^{-TR/T_1}) \tag{5.18}$$

and for *inversion recovery*

$$M_z(TI) = M_0(1 - 2Ae^{-TI/T_1}), \tag{5.19}$$

where the factor $A \approx 1$, depending on the sample inhomogeneity and the perfection of the 180°-pulse.

For the measurement of T_2 relaxation time, the *single spin echo* sequence has been extensively used. Saturation with a 90°-pulse is followed by a 180°-pulse after a time $TE/2$. In this time the phase coherence of spins has been disturbed by T_2 relaxation processes, static field inhomogeneities and very fast processes leading to motional narrowing. The 180°-pulse, also known as the *refocusing pulse*, will eliminate the effect of static field inhomogeneities in the following signal, but conserve the T_2 effects due to their random nature. The signal acquired after a $90° - TE/2 - 180° - TE/2$ scheme is called a *spin echo* providing the name for this sequence. With several TEs, the time constant can be solved by using equations (5.11)-(5.12) in the rotational frame of reference

$$M_{x,y}(TE) = M_{x,y}(0)e^{-TE/T_2}. \tag{5.20}$$

It is noteworthy that in biomaterials, multi-component T_2 relaxation times may be present, and are typically accounted for by adding several relaxation terms similar to that on the right hand side of (5.20). Also the time-scale of selected TEs is critical for detecting these components.

In MRI, data is acquired by spatial phase- and frequency-encoding of spin populations. The *free induction decay* data, known as the *k-space*, is converted to a magnitude image by applying a two-dimensional finite Fourier transform to the original data. The imaging sequences corresponding to the description of relaxation measurement above have the particular features supplemented with appropriate imaging field gradients, as shown later in Fig. 7.2.

5.2 Relaxation in articular cartilage

5.2.1 T_1 and T_2 relaxation

In an NMR sense, articular cartilage is a unique tissue since it consists both of a highly ordered collagen network and charged hydrophilic PGs that indisputably contribute to the relaxation properties of MRI-visible water protons.

Structural organization of water in anisotropic tissues can provide a powerful T_2 relaxation mechanism. Orientational dependence of T_2 in tendons, arising from the structural anisotropy of collagen, was first demonstrated by Berendsen (1962) and hence has been studied at different hydration levels [20, 53, 125]. The laminar appearance of articular cartilage was initially observed by Lehner *et al.* (1989) [89]. They claimed that the anisotropic T_1 and T_2 relaxation times in cartilage would be due to the spatial variations in the water content. Modl *et al.* (1991) first observed the low signal intensity (SI) in the superficial cartilage and linked the anisotropic appearance to the different histologic zones with variable collagen orientation [113]. Rubenstein *et al.* (1993) finally showed that SI from cartilage was dependent on the orientation of collagen fibrils in the B_0 field. By rotating bovine

patellae in the static field they demonstrated that the maximum signal was observed at an angle of 55°, *i.e.* the magic angle [132]. Other explanations included claims of SI dependence on PG concentration [124], truncation artefacts as the origin of laminar appearance [43, 48], and even a weak relation between the MR laminae and histologic zones has been presented [152]. Nevertheless, high-resolution rotational experiments confirmed that the T_2 contrast of cartilage is ultimately affected by the varying orientation of the collagen fibrils in the magnetic field [110, 161, 62, 159, 34]. It was recently argued that the magic angle effect would not alone account for the regional differences in T_2 *in vivo* [115]. To date, several studies have looked at the variation of T_2 in different species and joints, in both normal and degenerated cartilage, [36, 58, 112, 160, 59, 61, 114, 115, 140], correlated T_2 with the biochemical content [45], and provided qualitative microscopic data to support their MR findings [132, 34, 62, 58, 49, 76, 112, 61, 59]. Apart from the work described in this thesis, only a single quantitative microscopic study exists that has correlated the collagen structure, as revealed by PLM, to spatial the variation of T_2 [164].

In cartilage, the T_2 anisotropy *in vitro* is currently explained by the change in the orientation of collagen fibrils. It has been hypothesized that PGs oriented by collagen fibrils would mediate this anisotropic T_2 effect [62, 159], or water could interact directly with the collagen fibril [20, 108, 86]. With articular surface perpendicular or parallel to B_0, superficial tissue shows a zone with low T_2 due to strong dipolar effects around tangential fibrils. T_2 increases when moving towards the intermediate zone with unarranged fibrils, and varies here only little when the sample arrangement with respect to B_0 is altered [159]. Finally lower values are again observed in the deep radial zone with effective dipolar interaction [62, 159, 164]. With a 55° rotation of the sample, the geometric factor determining the dipolar interaction, equation (5.17), is minimized and higher T_2 values are observed in the superficial and deep tissue. Often the narrow band of low T_2 values in superficial tissue is not observed due to inferior imaging resolution as compared to high field MR-microscopy. In high field studies, an additional lamina of high T_2 is sometimes observed in deep tissue [61, 160]. T_1 and T_2 relaxation times of cartilage are strongly affected by osmotic loading [95] and mechanical compression [131, 74, 61], and are related to the outflow of water and rearrangement of the collagen network. T_1 relaxation time possesses no orientational dependence in cartilage [69] and has been reported to be relatively constant across the tissue [162, 110, 159]. Its role in terms of cartilage constituents remains to be clarified.

Spin density (SD) is obtained as a by-product from either T_1 or T_2 measurements, as the term M_0. MRI would seem to be ideal for the determination of cartilage water content, which is significantly altered during the disease process [99]. This is hampered, however, by several factors. First, SD measurements are always relative and therefore would require external phantoms to calibrate SD from tissue to actual water content [137]. Second, the solid matrix density needs to be taken into account

[137]. Third, relaxation processes affect the calculated SD, especially fast T_2 decay, and therefore compensation for these factors is required [111, 137]. Even after these procedures, the measured SD reflects the MRI-visible spin population, and thus does not necessarily account for all water compartments. The water content has been related to tissue T_2 relaxation time [94], however, the strong dependence of T_2 on collagen anisotropy through dipolar interaction is likely to contribute to the measured T_2 values, as discussed above.

Out of these native MR parameters, T_2 relaxation time has been most widely exploited. T_1 is non-specific for cartilage components and its role is somewhat unclear, and SD measurements may be prone to error.

5.2.2 Contrast agent-enhanced MRI

Paramagnetic contrast agents are frequently utilized in MRI to induce a relative enhancement of tissue SI. The paramagnetic center of contrast agents, often a gadolinium-atom embedded in an inert chelate, has a large and fluctuating local magnetic field that provides an additional relaxation sink for ^{1}H protons [87]. If other interactions are negligible, proton relaxation rates are functions of the contrast agent concentration C in tissue and relaxivity R [141, 21]

$$\frac{1}{T_{i,c}} = \frac{1}{T_{i,0}} + CR_i, \qquad i = 1, 2 \tag{5.21}$$

i.e. for the contrast agent concentration

$$C = \frac{1}{R_i}\left(\frac{1}{T_{i,c}} - \frac{1}{T_{i,0}}\right), \qquad i = 1, 2 \tag{5.22}$$

where $T_{i,0}$ and $T_{i,c}$ are the relaxation times in the absence and presence of the contrast agent, respectively. The relaxivity of the contrast agents is characteristic for different tissues and typically decreases with increasing magnetic field strength [37, 138, 165].

MR contrast agents have been utilized in qualitative *in vivo* imaging of articular cartilage for several years. Intra-articular and intravenous administration of agents has initially been used to increase T_1 contrast between tissues and synovial fluid, referred to as MR arthrography [31, 157]. Recently a quantitative technique, Gd-DTPA -enhanced T_1 imaging of articular cartilage, has been introduced [16, 17]. This technique utilizes the double-negative charge of the contrast agent, gadolinium diethylene triamine pentaacetic acid (Gd-DTPA). Analogous MRI approaches have been taken with the cationic contrast agents manganese [84] and nitroxide [12]. In Gd-DTPA -enhanced T_1 imaging, the contrast agent is assumed to distribute into cartilage inversely to the concentration of negatively charged GAGs and according to Donnan equilibrium, (2.2). The T_1 relaxation time shows an approximately linear

relationship with the GAG content of cartilage [16]. Further, if the relaxivity of the tissue is known or may be assumed, consecutive T_1 relaxation time measurements in the absence and presence of the contrast agent permit the estimation of the contrast agent concentration in the tissue using (5.22). For bulk cartilage studies, Bashir *et al.* (1996) derived a quasi-theoretical expression for FCD, exploiting the MRI-resolved contrast agent concentration [16]

$$\mathrm{FCD} = 2[\mathrm{Na}^+]_b \left(\sqrt{\frac{[\text{Gd-DTPA}^{2-}]_t}{[\text{Gd-DTPA}^{2-}]_b}} - \sqrt{\frac{[\text{Gd-DTPA}^{2-}]_b}{[\text{Gd-DTPA}^{2-}]_t}} \right), \tag{5.23}$$

where subscripts t and b stand for tissue and bath, respectively. This approach has been validated with ^{23}Na NMR and biochemical assays [16, 17], and thus proved to be applicable for *in vitro* assessment of bulk cartilage FCD. For *in vivo* studies, however, the equilibrating concentration in serum and synovial fluid is not known and thus the applicability of MRI-resolved FCD is limited. The technique has been used *in vitro* [16, 17, 150, 112] and its feasibility to follow GAG replenishment in cartilage explants has been successfully utilized [3]. Several *in vivo* investigations measuring T_1 relaxation time after intravenous or intraarticular administration of Gd-DTPA have been published [16, 15, 150, 149]. Protocol issues on delayed gadolinium enhanced MR imaging of cartilage (dGEMRIC) were recently published [28], and the technique has been applied to monitor PG distribution in patients with autologous chondrocyte transplants [55]. The ability of the technique to indicate the spatial, depth-dependent PG content of cartilage has not yet been demonstrated. In quantitative terms, the accuracy of the technique was recently questioned in a study that revealed the dependence of relaxivity on the macromolecule content in various protein models at $B_0 = 1.5$T, however cartilage was not studied [145]. Despite this, the overall sensitivity of the technique has been reported to be high [56].

5.2.3 Other quantitative MRI techniques

Several other MR techniques have lately been developed and tested for compositional characterization of articular cartilage. Magnetization transfer (MT) is a process in which the irradiation of macromolecular protons causes the saturation of the steady-state magnetization of the observable water pool interacting with the macromolecules [68]. Cartilage exhibits considerable MT effects due to the presence of abundant macromolecules and their interaction with water. Collagen has been reported to provide the main mechanism for MT in cartilage, while PGs may also contribute to the effect [77, 60, 135, 155]. $T_{1\rho}$ relaxation, *i.e.* spin-lattice relaxation in the rotating frame, provides a probe for studying macromolecules with slow rotational motion. In cartilage, $T_{1\rho}$ and $T_{1\rho}$ dispersion are sensitive to PGs, while their specificity to PGs remains open to debate [40, 1, 39, 38]. NMR-assessment of diffusion in cartilage is well supported by the importance of fluid flow in cartilage

during locomotion. The apparent diffusion coefficient (ADC) increases with PG and collagen depletion [27, 163], and ADC has been related to degenerated human cartilage *ex vivo* [49]. As described in Section 2.1.2, the negative FCD of cartilage attracts Na^+ ions. Thus, imaging of the ^{23}Na provides an alternative means for indirect quantitation of PGs [91]. Recent studies have described the sensitivity of the technique to reveal experimental PG-depletion [130], sodium concentration mapping in human cartilage *in vivo* [130] and the spatial variation of Na concentration [136].

The *in vivo* measurements of cartilage thickness and volume are a branch of their own. By the use of fat-supressed gradient echo imaging these measurements describe reproducibly both tissue loss in disease and topographical variations in normal human cartilage thickness [144, 41, 70].

Chapter VI

Aims of the present study

Quantitative MRI provides a probe to examine tissue water that interacts with the macromolecular environment, thus giving information on tissue which is inaccessible with any other modality. Specifically, ^{1}H NMR relaxation parameters potentially may provide information on the structure and composition of articular cartilage *in vitro* and *in vivo*. It is hypothesized that even the mechanical status of cartilage may be indirectly estimated since tissue mechanical properties are determined by the constituent macromolecules and their interactions with each other and the interstitial water. Currently, however, the relationship between MRI contrast and the spatially anisotropic ECM of cartilage is not adequately understood. To elucidate this dependence and the potential of MRI techniques to access mechanical characteristics of tissue, the present *in vitro* and *in vivo* studies particularly aimed to

- investigate the effect of selective enzymatic degradation of cartilage constituents on the T_2 relaxation time, and the parallel change in the tissue compressive stiffness;
- assess the spatial variation in T_2 relaxation time in cartilage and correlate it with the anisotropy of the collagen network;
- evaluate the capability of Gd-DTPA -enhanced T_1 imaging to reveal the spatial PG content of normal articular cartilage and after enzymatic PG depletion of superficial tissue;
- study whether the structure and composition of cartilage, as assessed by T_2 relaxation time and Gd-DTPA -enhanced T_1 imaging, could provide information on the mechanical characteristics of normal bovine articular cartilage;
- apply the dGEMRIC technique in (*i*) asymptomatic volunteers, and (*ii*) patients with autologous chondrocyte transplantation (ACT) and compare the

results with those from arthroscopic stiffness measurements.

Chapter VII

Materials and Methods

The present work consists of four studies (I-IV) supplemented with unpublished data. The study construction is summarized in Table 7.1.

Table 7.1: Summary of materials and methods

Study	Materials	n	MRI	Microscopy	Mech.Analysis
I	normal and digested bovine patellar osteochondral specimens	31	T_2, SD, T_1	PLM, DD	indentation E_s
II	bovine patellar osteochondral specimens	8	T_2	PLM, DD	-
III	macromolecular phantoms	35	R	-	-
	normal and digested bovine patellar cartilage	16	T_1, $T_{1\mathrm{Gd}}$ [Gd-DTPA]	DD	-
IV	bovine humeral and patellofemoral cartilage	32	T_1, $T_{1\mathrm{Gd}}$ [Gd-DTPA], T_2	-	unconfined compression ν, E_s, E_d, H_a
unpublished data	healthy volunteers	6	dGEMRIC	-	-
	patients with ACT	4	dGEMRIC		arthroscopic indentation

dGEMRIC: delayed Gadolinium Enhanced MRI of Cartilage, DD: digital densitometry, E_d: dynamic modulus, E_s: Young's modulus, H_a: aggregate modulus, PLM: polarized light microscopy, R: relaxivity of Gd-DTPA, SD: spin density, ν: Poisson's ratio.

7.1 Materials

7.1.1 Cartilage explants

For studies I and II, intact patellofemoral joints of 1-3-year old bovine were obtained from the local abattoir (Atria Lihakunta Oyj, Kuopio, Finland) within a few hours of slaughtering. Cylindrical osteochondral specimens ($n = 31$) were harvested from the lateral upper quadrant of each patella (Fig. 7.1, PAT) using a 13-mm hollow drill bit. The plug was detached with a saw (Stryker Autopsy Saw 868, Stryker Europe bv, Uden, The Netherlands). Articular cartilage with 1-2 mm of subchondral bone was isolated using a diamond saw (Buehler Isomet Low Speed Saw, Buehler Ltd., Lake Bluff, IL, USA). Zero hour control specimens ($n = 9$) were investigated immediately after preparation (I, II). For study I, the rest of the samples were incubated with or without enzymes for 44 hours at +37°C and 5% CO_2 in Gibco BRL Minimum Essential Medium with Earle's salt (Life Technologies, Paisley, Scotland, UK) supplemented with 100U/ml penicillin (PAA Laboratories, Linz, Austria), 100 mg/ml streptomycin (Sigma Chemical Company, St. Louis, MO, USA), 70 mg/ml L-ascorbic acid (Sigma) and 200 ml L-glutamine (PAA Laboratories). The 44-hour control samples ($n = 7$) were incubated without enzyme supplementation. To digest the superficial collagen network of samples ($n = 8$), 30 U/ml of type VII bacterial collagenase (Sigma) was added, and to deplete PGs from samples ($n = 7$) 0.1 U/ml chondroitinase ABC (Seikagaku Corp., Tokyo, Japan) was used. Finally, a 6-mm osteochondral disk was removed from the center of the original sample with a steel punch to assure that the enzyme penetration into the specimen took place only through the articular surface into the deeper tissue.

In study III, patellofemoral joints were stored overnight at +5°C after slaughtering. Cartilage disk pairs (dia. = 4mm, $n = 8$) without subchondral bone were prepared from the lateral upper-quadrant of the patellae using a 4-mm biopsy punch (Stiefel Laboratories Ltd., Sligo, Ireland). One disk served as a control while the other was treated with chondroitinase ABC for 44 hours as described previously. Prior to MRI measurements, a small slice of tissue was cut from the side of each sample for DD measurements.

In study IV, humeral and patellofemoral joints were stored overnight and two adjacent samples without subchondral bone (dia. 3 and 4mm, $n = 32$) were prepared from various sites of the joints (Fig. 7.1, all locations). Prior to measurements, all samples were equilibrated for a minimum of one hour in phosphate buffered saline solution (PBS) without Ca^{2+} or Mg^{2+} (HyClone Europe Ltd., Cramlington, UK and Life Technologies, Paisley, Scotland, UK).

7.1.2 Macromolecule phantoms

For relaxivity experiments (III), Gd-DTPA (Aldrich Chemical Company, Milwaukee, WI, USA) solutions (0, 0.12, 0.25, 0.5, 1, 2 and 5mM) in PBS were prepared.

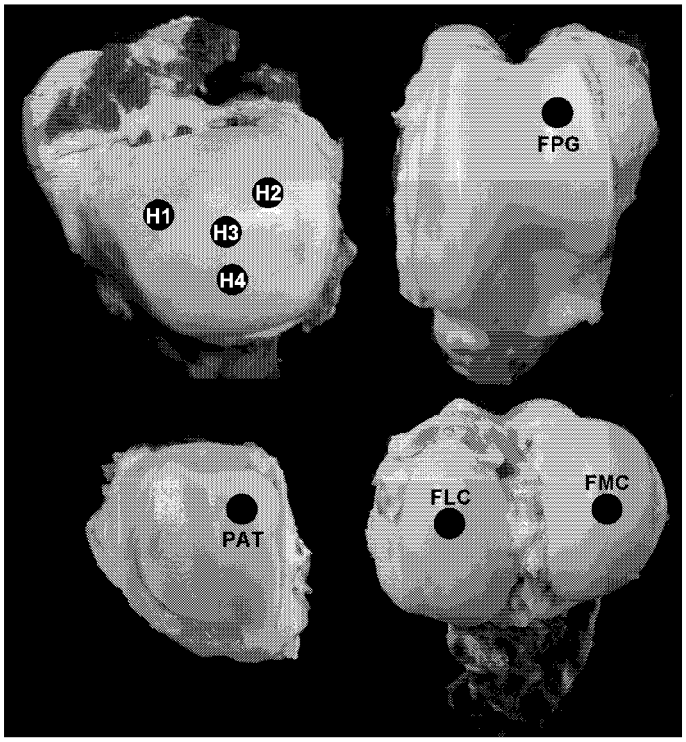

Figure 7.1: Anatomical sites for the samples from different bovine articular surfaces. Humeral samples: anterior (H1), posterior (H2), central (H3) and proximal (H4); patellofemoral samples: lateral upper quadrant of the patella (PAT); femoral patellar groove (FPG), femoral lateral condyle (FLC) and femoral medial condyle (FMC).

Different amounts of skimmed milk powder (Valio Ltd., Helsinki, Finland) were added into these stock solutions to obtain contrast agent solutions with 0, 10, 20, 30 and 40% of solid skimmed milk by weight, chosen to cover the approximate range of the macromolecules in healthy human articular cartilage at different depths (about 20% in superficial tissue to 35% in deep tissue [22].

7.1.3 Healthy volunteers and ACT patients

Asymptomatic volunteers (age 39±11, 3 female and 3 male) and patients undergoing an ACT surgery in medial or lateral femoral condyles 12-19 months earlier (age 28± 12, 4 male) were studied according to the dGEMRIC protocol [28]. An intravenous injection of 0.2mM/kg Gd-DTPA (Magnevist, Schering AG, Berlin, Germany) was followed by 10 minutes of knee bending exercises to speed up the contrast agent

intake. MR experiments were carried out within 2 - 3 hours after the injection.

7.2 MRI methods

7.2.1 T_2 relaxation time measurements

T_2 relaxation time of osteochondral samples (I, II) and excised cartilage disks (IV) was determined in PBS solution using 5-mm or 16-mm high resolution spectroscopy probes (Varian Associates Inc., Palo Alto, CA, USA), respectively. A 9.4T vertical magnet (Oxford 400 NMR, Oxford Magnet Technology, Oxford, UK) and a SMIS console (SMIS Ltd., Surrey, UK) equipped with Magnex gradients (30G/cm, Magnex Scientific Ltd., Abingdon, UK) was utilized at 25°C. T_2-weighted experiments were performed using a single spin-echo sequence (Fig. 7.2) with adiabatic refocusing [54] and minimized sensitivity to diffusion [50], with four echo times (TE = 14, 24, 34, 44ms), a repetition time (TR) of 2500ms and a 1-mm slice. The frequency-encoding direction was selected along the cartilage thickness, and the cartilage surface was aligned perpendicular to the B_0 field.

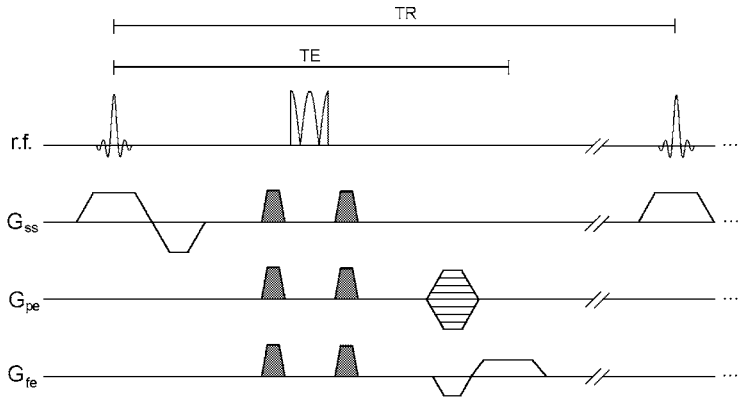

Figure 7.2: Timing diagram of the single spin-echo imaging sequence used in the experiments. For T_2 measurements the echo time (TE) is varied while for saturation recovery T_1 measurements repetition time (TR) is altered. For inversion recovery T_1 meaurements the sequence is preceded by an inversion pulse. G_{ss}, G_{pe} and G_{fe} stand for slice selection, phase encoding and frequency encoding gradients, respectively. 90°-pulse is slice selective while refocusing with 180°-pulse is achieved using a non-selective adiabatic BIR-4 pulse [54]. Crusher gradients (indicated in gray) destroy residual magnetization from incompletely refocused spins.

For studies I and II, a 256×128 data matrix was acquired and zero-filled to 256×256. With a 20-mm field of view (FOV), an in-plane resolution of 78×78μm was obtained. For study IV, a 256×64 data matrix was collected, yielding a 39μm resolution along the cartilage depth. T_2 relaxation time maps were calculated using least-squares fitting (Matlab, Mathworks Inc., Natick, MA, USA) into the linearized form of (5.20). Consequently, depthwise T_2 relaxation time profiles were calculated after averaging several pixels along the cartilage surface. SD maps were calculated by extrapolating the T_2 fit to $TE = 0$ms (I).

7.2.2 Measurements of Gd-DTPA relaxivity

Gd-DTPA relaxivity per kilogram of water was determined for the contrast agent solutions containing varying amounts of skimmed milk powder ($n = 35$). Measurements were performed at 9.4T using a spectroscopic inversion recovery T_1 series (11 TIs between 20-4000ms, $TR = 10000$ms). Relaxivity was determined by fitting T_1 and contrast agent concentration data into (5.22).

7.2.3 T_1 and Gd-DTPA -enhanced T_1 measurements

In study I, T_1 relaxation time of two samples in each group (control, chondroitinase ABC, collagenase) was measured with the same setup as in Section 7.2.1 but using an inversion recovery spin-echo sequence (TE = 14ms, TR = 6000ms, TI = 50, 150, 500, 800, 1000ms). T_1 relaxation time maps were obtained by performing a three-parameter fit into (5.19). T_1 profiles were calculated as described in Section 7.2.1.

In study III, the appropriate diffusion time for Gd-DTPA to penetrate into 4-mm cartilage disks ($n = 6$) was studied by performing successive T_1-weighted saturation recovery experiments ($TE = 14$ms, $TR = 800$ms) with adiabatic refocusing immediately after immersion in 1ml of 1mM Gd-DTPA solution for six hours.

For studies III and IV, Gd-DTPA -enhanced T_1 imaging was conducted with the following protocol. A T_1-weighted saturation recovery series (TE = 14ms, TR = 200, 500, 1000, 1500, 3000, 5000ms) was measured with a saturation recovery sequence. This experiment was followed by an equilibrating period of at least 2.5 hours in 1mM Gd-DTPA solution. Finally, another T_1-weighted imaging series (TE = 14ms, TR = 100, 300, 500, 800, 1200, 1500ms) was conducted. T_1 relaxation time maps and profiles were calculated as earlier. Spatial Gd-DTPA concentration profiles were calculated from T_1 and $T_{1\mathrm{Gd}}$ profiles using (5.22).

7.2.4 dGEMRIC of normal and ACT-repaired cartilage

Single slice T_1-weighted experiments were conducted with 1.0T clinical MRI scanners (Siemens Harmony or Siemens Impact Expert, Erlangen, Germany), using a fast inversion recovery sequence (seven TIs between 25 and 1600ms, TE = 15 or

30ms, TR = 2000ms, 512 × 512 matrix, FOV = 230 or 290mm, 2 or 3mm slice thickness). Images were obtained in two planes (medial and lateral oblique sagittal slice positioning for healthy volunteers, sagittal and coronal orientations for ACT patients). T_1 maps with contrast agent were fitted and $T_{1\mathrm{Gd}}$ profiles were calculated by averaging an area along the articular surface, corresponding to the slice thickness.

7.3 Microscopic techniques

7.3.1 Polarized light microscopic measurements

For studies I and II, the samples were prepared for microscopy after MRI and biomechanical measurements. Each sample was cut into two halves in a vertically randomized direction. The samples for PLM were fixed with formalin, decalcified, embedded in paraffin [8, 78], and cut into 5-μm sections. For DD of cartilage PGs, Safranin-O -stain (Fisher Scientific, Fair Lawn, NJ, USA) was added into formalin to minimize PG loss during fixation [79]. Three-micrometer thick microscopic sections were processed and stained with Safranin-O [80]. The PLM analysis of the collagen network was performed using a Leitz Ortholux BK-2 polarized light microscope (Leitz Wetzlar, Wetzlar, Germany) equipped with a 6.3× magnifying strain-free objective, a cooled 12-bit CCD-camera (Photometrics, Tucson, AZ), and crossed polarizers. Monochromatic light ($\lambda = 589 \pm 10$nm) was used.

Grayscale microscopic images (pixel size 3.6×3.6μm) with 0 and 45° arrangement of polarizers against the tangential zone were recorded. The images were combined (see Section 3.1) from the cartilage surface to subchondral bone using a 627-μm-wide area, and were converted to BF. Because orientational dependence of fibrils also exists in the plane of vertical sectioning, four vertically randomized orientations were analyzed. Three 5-μm-sections, in each orientation, were measured to minimize the effect of variable section thickness. For each section, a depthwise BF profile was obtained by averaging data parallel to the cartilage surface, and the final profile was calculated as an average of all sections in all orientations. Due to the different orientations and finite section thickness, the final profile received contributions from the three-dimensional matrix instead of a single plane.

7.3.2 Digital densitometry of Safranin-O -stained proteoglycans

To determine the OD distribution of Safranin-O in samples (I, II, III), the aforementioned camera and optics adjusted to standard transmission mode, equipped with a four times magnifying objective (pizel size 5.7 × 5.7μm) were used with monochromatic light ($\lambda = 492 \pm 5$nm). The system was calibrated between 0 and 3.6 absorbance units using a neutral density filter set (Schott, Mainz, Germany). For each sample, six 3-μm-sections were analyzed, full thickness profiles were calculated from a 110 pixels wide area and averaged.

7.3.3 Kossa's staining

Kossa's staining for calcium was used to reveal possible calcified tissue in cartilage sections (III). In the technique, silver nitrate binds to calcium salts, which after exposure to ultraviolet light appears dark [96].

7.4 Mechanical measurements

For mechanical measurements, a custom built high-precision material testing device was used. The device consisted of a precision motion controller (Newport PM-500-C, Newport, Irvine, CA, USA), 10 or 100N load cells (Sensotec, Columbus, OH, USA) and a custom-programmed (Labview, Austin, TX, USA) acquisition and analysis software [151].

7.4.1 Static loading

In study I, Young's modulus was determined for samples using a stepwise stress-relaxation experiment in indentation geometry. The sample was compressed with a porous cylindrical indenter (dia. = 1.0mm) by a strain of 20% with ten steps of equal size. The compression speed was 1μm/s and an 8-min relaxation was allowed between each step to reach equilibrium. The indenter force and displacement were registered during the measurement. Cartilage tissue was modeled as a linearly elastic material bonded to rigid subchondral bone, equation (4.2), to calculate Young's modulus from the equilibrium response in the linear range. A typical value $\nu = 0.1$ was used in the calculations [72, 11]. The original thickness of the cartilage, essential for the experimental testing and data reduction, was obtained using high frequency ultrasound [73, 151] and needle-probe measurements [73].

In study IV, a single-step stress-relaxation experiment was conducted in unconfined geometry. An equilibrium compression corresponding to 10% strain was followed by a step of 5% strain at 1μm/s. A 30min relaxation period was allowed. Young's modulus was determined from the equilibrium response. Poisson's ratio for the samples was determined optically with the same loading protocol as used for the modulus measurements [72]. The aggregate modulus was calculated from (4.5) using the measured E_s and ν.

7.4.2 Dynamic loading

In study IV, static experiments were followed by 1Hz dynamic loading. Cartilage disks equilibrated at 15% strain were loaded with four sinusoidal cycles of 1% strain amplitude. The dynamic modulus was calculated from the last two cycles as the ratio of peak-to-peak stress and strain.

7.4.3 Arthroscopic indentation

For ACT patients, *in vivo* mechanical measurements were conducted using an arthroscopic indentation device (Artscan 1000, Artscan Ltd, Espoo, Finland) [98] within three weeks from T_1 mapping. In this technique, the cylindrical indenter (dia. = 1mm, length = 0.3mm) of the device was pressed instantaneously against the cartilage surface and the resisting force was registered to indicate tissue indentation stiffness in Newtons. Measurements were performed from (*i*) the repair site and (*ii*) from a control site at the corresponding site of the other femoral condyle. The $T_{1\mathrm{Gd}}$ values of approximately same locations were compared.

7.5 Statistical analysis

In study I, the nonparametric Mann-Whitney U-test was used in the statistical comparison of T_2, spin density, Young's modulus and cartilage thickness data between different sample groups.

For study II, downsampling of BF profiles to match MRI resolution with nearest neighbor interpolation (Matlab) enabled the linear Pearson correlation analysis between surface-matched T_2 and $1/BF$ datasets from cartilage surface to subchondral bone for each sample, and for pooled data of all samples. The additional contribution of PGs, as measured with DD was assessed with stepwise linear regression analysis (SPSS, SPSS Inc., Chicago, IL). In the analysis, first $1/BF$ and thereafter OD were entered into a linear model to assess whether accounting for PGs would provide a significant improvement to the correlation with T_2.

In study III, superficial $T_{1\mathrm{Gd}}$ and MRI-resolved [Gd-DTPA] were compared between the control and PG-depleted superficial tissue using the Wilcoxon signed-ranks test for two related samples. To reveal the relationship between MR parameters and DD, linear Pearson correlation analysis between resampled and surface-matched MRI and microscopic data was performed. To test whether [Gd-DTPA] would provide a more useful tool for estimating the GAG content than T_1 in the presence of Gd-DTPA, the Wilcoxon signed-ranks test was used to compare the absolute values of correlation coefficients between OD and $T_{1\mathrm{Gd}}$ or [Gd-DTPA] in normal and enzymatically treated samples. To further test the spatial matching of MRI parameters and OD, the depthwise MR and microscopic data was divided into more superficial and deep data by successively moving the cut point (pixel) of the two data sets into deeper tissue. Consecutively, the linear Pearson correlation coefficient, slope and intercept were tested for the two data sets to reveal the tissue depth at which the MR parameters did not follow the PG content, as judged by the assumption of a linear OD-MR parameter relationship. At this depth, the Wilcoxon test was applied to compare the slope and intercept of more superficial or deeper data between control and enzymatically degraded samples.

In study IV, biomechanical and MR parameters were correlated with linear Pearson correlation analysis. Forward linear regression analysis was used to reveal whether a combination of MR parameters could further improve the correlation between relaxation and mechanical properties. The Friedman test for several dependent samples and the Friedman post-hoc test were applied to assess the topographical variation in MR and biomechanical parameters, and to reveal whether MRI could distinguish between mechanically different tissue.

For the *in vivo* experiment with healthy volunteers, the Wilcoxon's signed-ranks test for two related samples was used to compare bulk $T_{1\mathrm{Gd}}$ values between the patella and femoral patellar groove for both lateral and medial sides.

Chapter VIII
Results

8.1 Quantitative MRI of normal and enzymatically degraded articular cartilage

Various MR parameters were studied in normal and enzymatically treated bovine patellar cartilage (I, III). The effects of enzymatic treatments were verified with PLM and/or DD microscopic techniques. The most important results are given in Table 8.1.

In study I, T_2 relaxation time increased significantly only after a 44-hour collagenase treatment (Fig. 8.1). Superficial SD was not altered by enzymatic digestions when compared to deeper tissue. T_1 relaxation time after the PG cleavage remained unchanged while the digestion significantly decreased $T_{1\mathrm{Gd}}$ and increased [Gd-DTPA] as compared to controls (Fig. 8.2) (III). No significant differences in cartilage thickness between sample groups were observed.

Table 8.1: Values of various MR parameters at 9.4T in normal and enzymatically treated superficial (0-78μm) bovine patellar cartilage (total thickness 1200-4100μm). Number of samples is given in parentheses.

Group	T_2 (ms)	T_1 (ms)	$T_{1\mathrm{Gd}}$ (ms)	[Gd-DTPA] (mM)
control (0h)	40±5 (9^{oc})	1590±180 (8^{c})	330±50 (8^{c})	0.51±0.09 (8^{c})
control (44h)	46±9 (7^{oc})	-	-	-
collagenase	358±133^{a} (8^{oc})	-	-	-
chondroitinase	42±13 (7^{oc})	1640±180 (8^{c})	300±80^{b} (8^{c})	0.61±0.12^{b} (8^{c})

^{a} $p < 0.01$, Mann-Whitney U-test, ^{b} $p < 0.05$, Wilcoxon signed ranks test
^{oc} osteochondral plug, ^{c} cartilage disk

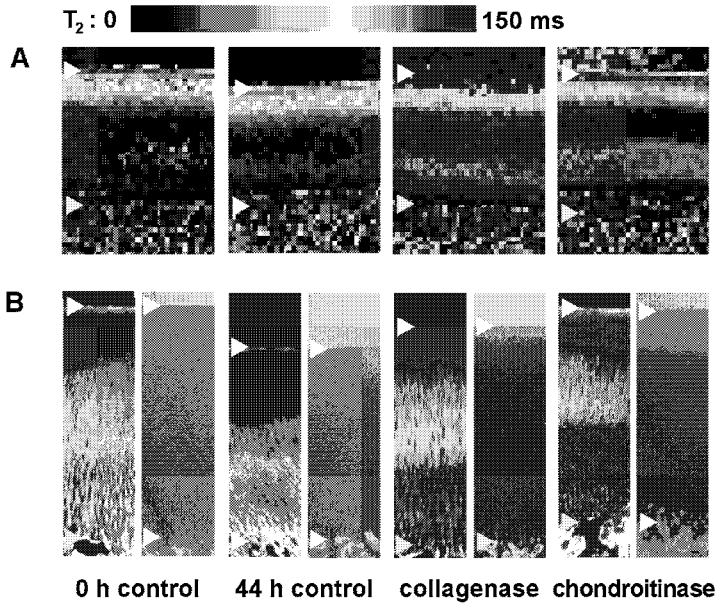

Figure 8.1: (A) T_2 maps at 9.4T, and (B) microscopic images (left: PLM image, right: DD image, 4× magnification) for representative control, collagenase digested and chondroitinase ABC treated bovine osteochondral specimens. White and yellow arrows indicate articular surface and cartilage-bone interface, respectively.

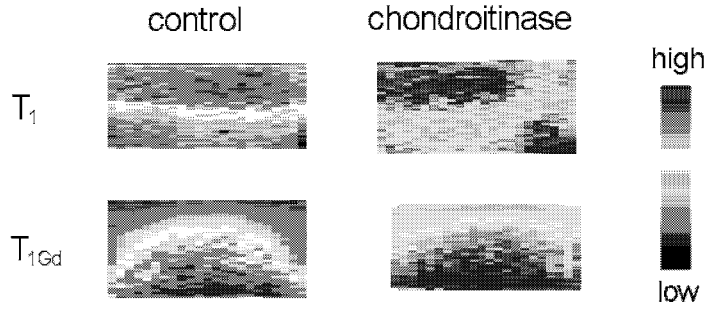

Figure 8.2: T_1 maps at 9.4T (left, color bar T_1 = 1000...2000ms) and T_{1Gd} maps (right T_1 = 200...600ms) for control and chondroitinase ABC treated bovine osteochondral specimens. Articular surface is towards the top of the page.

8.2 Spatial MR-assessment of cartilage structure and composition

Spatial T_2 profiles were assessed and compared to PLM and DD measurements (II). A typical trilaminar T_2-appearance was observed, often with an additional maximum close to the cartilage-bone interface. Visually, PLM images appeared similar to T_2 maps although inverted, with a hyperintense appearance of arranged collagen fibrils in the superficial and deep zones, and a hypointense signal in the intermediate zone with its unorganized fibril structure. Analogously to the T_2 maxima often present in deep cartilage, a hypointense region was seen in PLM images. Correlation analysis revealed a linear relationship with $r = 0.907 \pm 0.020$ between T_2 and $1/BF$ among samples (Fig. 8.3), and $r = 0.789$ with pooled data from all samples. Stepwise linear regression analysis revealed a minor, yet significant improvement in the Pearson correlation coefficient after adding OD into the linear model (for pooled data $\Delta r^2 = 0.04$).

To understand Gd-DTPA relaxivity at 9.4T (III), the relationship between Gd-DTPA relaxivity and macromolecular content was assessed in a simple skimmed milk solution model. Relaxivity increased with macromolecular content (Fig. 8.4), however, this was less dramatic as compared with the finding at a lower field strength [145].

Spatial $T_{1\mathrm{Gd}}$ and [Gd-DTPA] profiles were assessed and compared with OD of Safranin-O -stained sections of normal and chondroitinase ABC-treated tissue (III). For these measurements, the appropriate balancing time for 4-mm cartilage samples in 1mM Gd-DTPA solution was found to be 2.5 hours.

Cartilage typically revealed a decrease in T_1 from superficial to deep cartilage, sometimes with low values close to the articular surface. Immersion in Gd-DTPA resulted in an overall shortening of T_1 relaxation time, with shorter values in superficial cartilage and longer values in deep tissue, resembling the spatial distribution of PGs in cartilage (Fig. 8.5). Correlation analysis revealed a linear positive relationship between $T_{1\mathrm{Gd}}$ and OD ($r = 0.885 \pm 0.015$ for control and $r = 0.893 \pm 0.028$ digested samples). For [Gd-DTPA] and OD the correlations were negative with $r = -0.915 \pm 0.014$ and $r = -0.931 \pm 0.023$, respectively. Further, the MR parameters showed a significant spatial correlation with OD in the more superficial tissue up to a depth of $60 \pm 15\%$ of total cartilage thickness, ranging from 34 to 89 %. Up to this depth, plotting $T_{1\mathrm{Gd}}$ against OD revealed an r of 0.964 ± 0.038 and -0.927 ± 0.061, a slope of 147 ± 38 and 130 ± 39, and an intercept of 288 ± 47 and 288 ± 27 for control and chondroitinase ABC treated tissue, respectively. Similarly, for [Gd-DTPA] and OD, r was 0.968 ± 0.025 and -0.930 ± 0.065 with a slope of -0.215 ± 0.064 and -0.230 ± 0.050, and an intercept of 0.690 ± 0.077 and 0.753 ± 0.063 for control and chondroitinase ABC treated samples, respectively. The slopes between control and chondroitinase treated groups were not statistically dif-

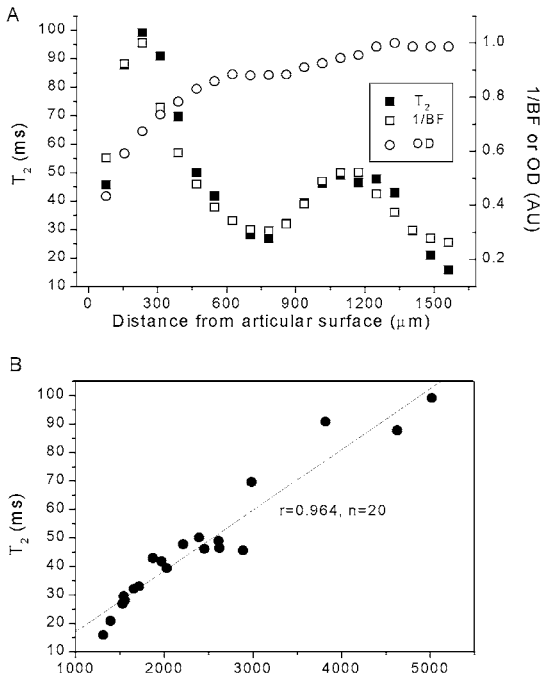

Figure 8.3: (A) T_2 and the reciprocal of optical birefringence ($1/BF$) as a function of cartilage thickness, and (B) linear relationship between these parameters for a representative sample.

ferent, while the intercept in the case of [Gd-DTPA] and OD differed statistically significantly between the two groups. The site where the anomalous behavior began did not match with any specific PG concentration as measured by DD, but occurred within a wide range of OD values in different samples. Kossa's staining did not reveal that any calcified cartilage could account for this finding.

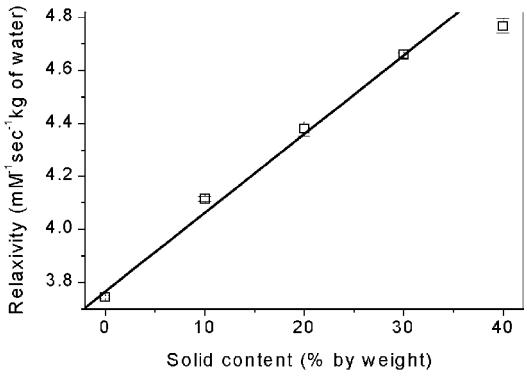

Figure 8.4: Relaxivity of Gd-DTPA at 9.4T with varying concentrations of skimmed milk powder in PBS.

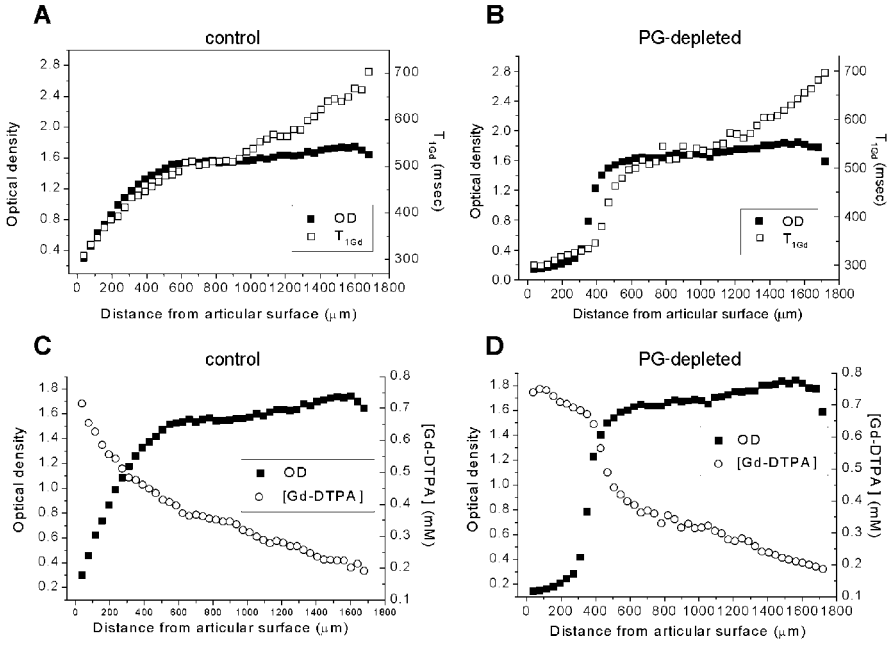

Figure 8.5: (A, B) $T_{1\mathrm{Gd}}$ profiles and (C, D) contrast agent concentration as a function of cartilage depth for control and PG-depleted tissue.

8.3 Quantitative MRI as an indicator of cartilage mechanical properties

Superficial and/or bulk T_2, $T_{1\mathrm{Gd}}$ and [Gd-DTPA] were related to tissue Young's modulus, aggregate modulus, dynamic modulus and Poisson's ratio in normal and enzymatically degraded bovine patellar cartilage harvested from various anatomical sites (I, IV). A typical load response of cartilage is shown in Fig. 8.6.

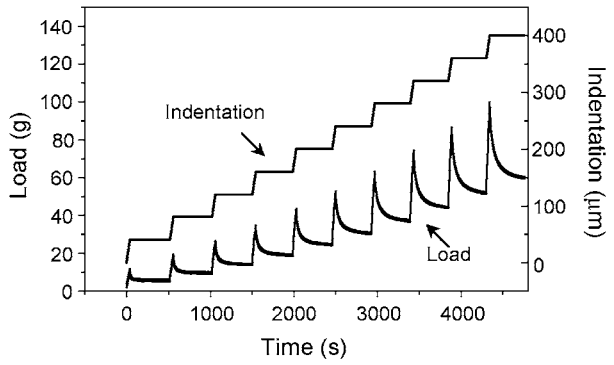

Figure 8.6: Load response of articular cartilage in a multi-step stress relaxation indentation experiment.

After the digestion of collagen or PGs, a statistically significant decrease in Young's modulus was observed (0h control: 1.07 ± 0.31MPa, 44h control: 1.09 ± 0.29MPa, collagenase: 0.67 ± 0.28MPa, chondroitinase ABC: 0.41 ± 0.28MPa). For MR parameters, only T_2 revealed a significant change after collagenase treatment (Fig. 8.7) (I). For normal bovine humeral and patellofemoral cartilage (IV), moderate to excellent correlations were established between mechanical and MRI parameters (Table 8.2). These correlations were especially high when a single articular surface, the proximal humerus, was assessed. Forward linear regression analysis of combined data from both humeri and patellofemoral joints revealed that a combination of [Gd-DTPA] or $T_{1\mathrm{Gd}}$ with the superficial T_2 improved the correlation with Young's modulus significantly ($p < 0.05$) with an average r improvement of 0.34 ± 0.15. Assessing the two different types of joints separately combining MR parameters did not improve the correlation coefficient statistically significantly.

MR parameters revealed topographical differences that often could be related to a similar pattern in mechanical properties (Fig. 8.8). For humerus, the Friedman test revealed statistically significant topographical differences in Young's modulus, aggregate modulus, Poisson's ratio, [Gd-DTPA] and $T_{1\mathrm{Gd}}$. For the patellofemoral

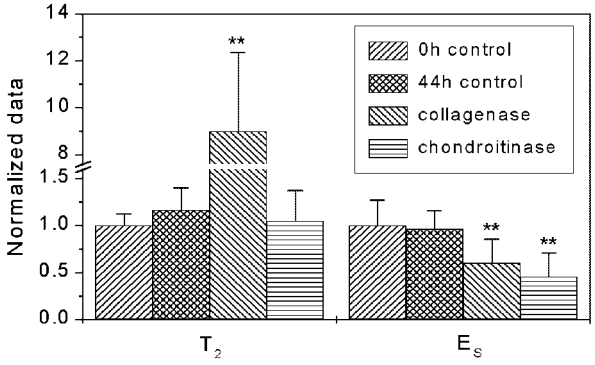

Figure 8.7: Superficial T_2 and Young's modulus in control and enzymatically digested sample groups, normalized by the mean 0h control value (** $p < 0.01$, Mann-Whitney U-test).

joint, the superficial T_2 relaxation time differed statistically significantly among the sites. A further Friedman post-hoc assessment indicated that [Gd-DTPA] and $T_{1\mathrm{Gd}}$ values were indicative of the consistent difference in Young's modulus between the anterior and central area of the bovine proximal humerus.

8.4 dGEMRIC of normal and ACT-treated cartilage

In healthy volunteers (Fig. 8.9A), the bulk $T_{1\mathrm{Gd}}$ values (mean value of tissue from surface to deep cartilage) in approximately adjacent compartments of the patella and femur were compared (Table 8.3). For both medial and lateral sides, a statistically significant difference ($p < 0.05$, Wilcoxon signed-ranks test) was observed, with 20% greater T_1 values for the patella. In the femur, $T_{1\mathrm{Gd}}$ values were higher on the lateral side as compared to medial tissue ($p < 0.05$). $T_{1\mathrm{Gd}}$ profiles revealed an increasing pattern of T_1 for most profiles (Fig. 8.10), consistent with the known fact that deep cartilage has a higher PG concentration than the superficial tissue.

In patients with ACT, arthroscopic examination revealed a good filling of the repair site. The MR assessment of the grafts was in agreement with this finding (Fig. 8.9B). Often a subchondral process was observed in MRI. ACT grafts revealed T_1 values of 91-164% relative to the control tissue (control: 310 ± 40ms, graft: 340 ± 60ms), suggesting that PG replenishment had occurred at the repair sites. However, the dynamic stiffness of the repair site was only 24-51% of the control tissue (control: 3.29 ± 0.79N, graft: 1.34 ± 0.38N), indicating that there was incomplete mechanical maturation of the grafts (Fig. 8.11).

Table 8.2: Linear correlation coefficients (r) between the MR and biomechanical parameters in bovine humeral and knee articular cartilage. MR parameters are for bulk tissue, except for $T_{2,s}$ that represents the superficial tissue (0 - 78μm).

	All ($n = 20$ or 32)	Humerus ($n = 8$ or 20)	Knee ($n = 12$)
T_1 *vs.* E_s	-0.118	-0.087	0.032
T_1 *vs.* E_d	-0.510	-0.433	-0.437
T_1 *vs.* H_a	-0.088	-0.139	-0.089
T_1 *vs.* ν	0.184	0.248	0.251
T_2 *vs.* E_s	-0.334	-0.208	-0.310
T_2 *vs.* E_d	-0.080	-0.050	0.202
T_2 *vs.* H_a	-0.342	-0.268	-0.327
T_2 *vs.* ν	0.217	0.631	0.225
$T_{2,s}$ *vs.* E_s	-0.674	-0.738	-0.624
$T_{2,s}$ *vs.* E_d	-0.470	-0.736	-0.128
$T_{2,s}$ *vs.* H_a	-0.650	-0.699	-0.617
$T_{2,s}$ *vs.* ν	0.530	0.608	0.450
$T_{1\mathrm{Gd}}$ *vs.* E_s	0.796	0.934	0.702
$T_{1\mathrm{Gd}}$ *vs.* E_d	0.348	0.681	0.192
$T_{1\mathrm{Gd}}$ *vs.* H_a	0.697	0.808	0.725
$T_{1\mathrm{Gd}}$ *vs.* ν	-0.282	-0.215	-0.441
[Gd-DTPA] *vs.* E_s	-0.861	-0.874	-0.843
[Gd-DTPA] *vs.* E_d	-0.643	-0.705	-0.468
[Gd-DTPA] *vs.* H_a	-0.735	-0.715	-0.853
[Gd-DTPA] *vs.* ν	0.381	0.325	0.636

Table 8.3: T_1 relaxation time (ms) values for healthy volunteers ($n = 6$) in different compartments of the patella and femoral condyles.

	medial	lateral
patella	330 ± 40	370 ± 40
femur	280 ± 40	310 ± 20

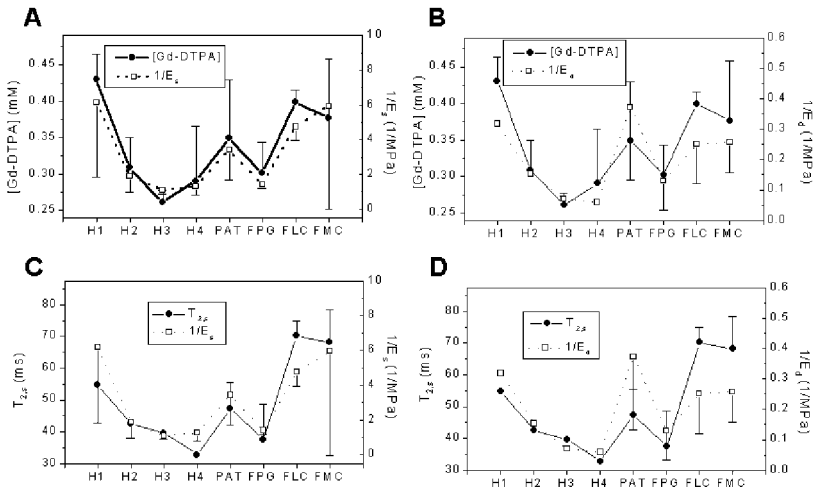

Figure 8.8: Topographical variation of bulk contrast agent concentration ([Gd-DTPA]) (A, B) and superficial T_2 relaxation time (C, D), with reference to the reciprocal values of Young's modulus (E_s) and dynamic modulus (E_d) ($n = 2 - 5$ per point). High [Gd-DTPA] and $T_{2,s}$ values are attributed to lower PG content and lower integrity of the superficial collagen network, respectively. Sample locations are described in Fig. 7.1.

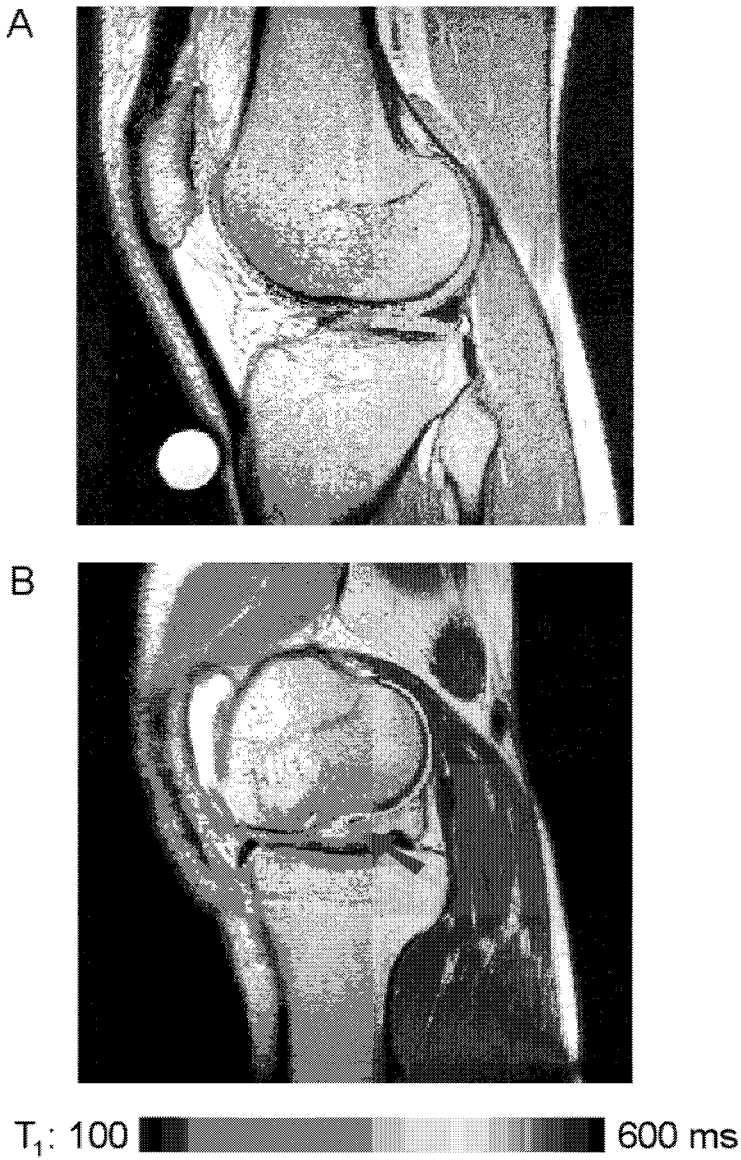

Figure 8.9: dGEMRIC T_1 maps at 1.0T: (A) for an asymptomatic volunteer articular cartilage reveals increasing T_1 values from superficial to deep cartilage (in-plane resolution 450 × 450μm), (B) map reveals high T_1 values in the ACT-graft (shown with the arrow) indicative of PG replenishment (in-plane resolution 570 × 570μm).

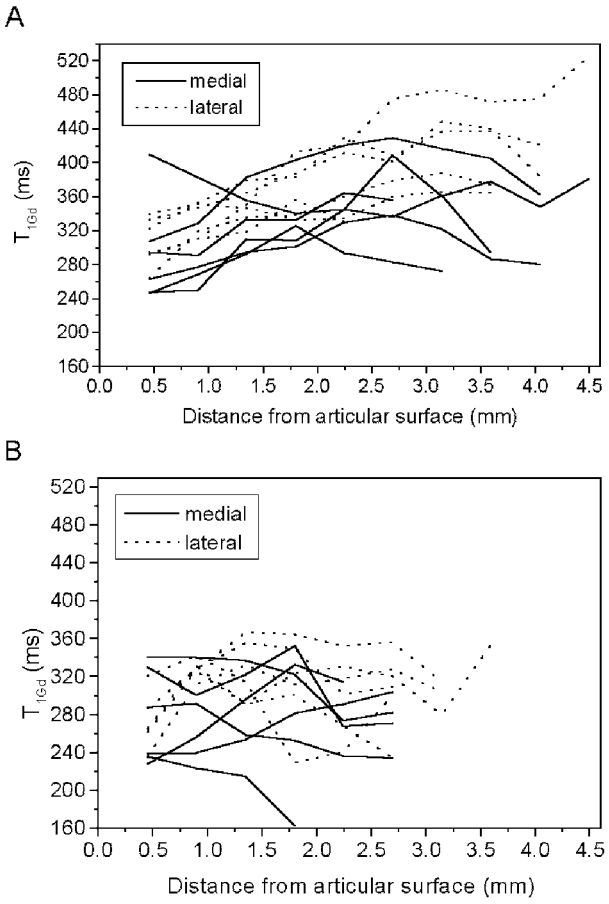

Figure 8.10: Spatial T_1 profiles in (A) patella and (B) femur of asymptomatic human subjects ($n = 6$). The resolution of data is 450μm.

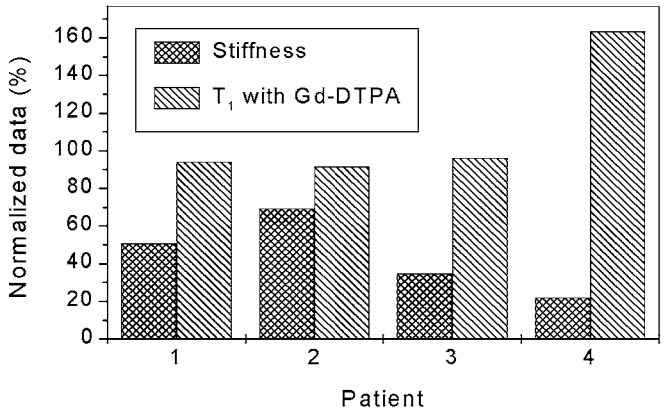

Figure 8.11: For four patients with ACT-surgery in the femoral condyle, arthroscopically measured dynamic stiffness and $T_{1\mathrm{Gd}}$ at 1.0T, normalized with the control value from adjacent condyle.

Chapter IX
Discussion

9.1 Quantitative MRI, cartilage structure and composition

Enzymatic degradation of cartilage components in superficial tissue confirmed that T_2 relaxation is sensitive to the integrity of the collagen network (I). Spin density and additional T_1 measurements suggested that the observed increase in T_2 was not likely to be due to an increase in the water content, but rather from the destruction of the collagen network and the consequent alteration in dipolar interactions. $T_{1\mathrm{Gd}}$ and [Gd-DTPA] were altered by the enzymatic cleavage of PGs, while T_1 without contrast agent did not follow the PG loss (II). The experimental results were in line with previous investigations indicating that the Gd-DTPA -enhanced T_1 imaging is applicable for detecting cartilage PGs and their loss [16, 17, 112, 150].

Spatial correlation of T_2 relaxation time, measured with the articular surface perpendicular to the B_0 field, and optical birefringence revealed that the spatial variation in T_2 is strongly controlled by the organization, *i.e.* anisotropy of the collagen network (II). This finding is in accordance with a very recent study that investigated anisotropic T_2 and the fibril angle as resolved from quantitative PLM measurements [164]. In the present study, a minor, yet significant, improvement to this correlation was achieved by accounting for PGs, suggesting that PGs may have a minor role in the formation of cartilage T_2 contrast (II), though PG cleavage did not alter the superficial T_2 relaxation time (I). Water [62, 94], collagen content [45] and the degree of compression [115] may also contribute to the absolute T_2 values. For a more realistic view of T_2 processes in cartilage, a deeper knowledge of relaxation mechanisms between different water compartments in cartilage is required. Since sample orientation relative to B_0 clearly affects the MR laminar appearance, laminar thickness may vary and MR laminae are not directly related to histological zones, although they are closely connected. Also, T_2 was investigated only with a single sample orientation, a fact that is to be considered as a limitation. Further *ex/in vivo* studies are necessary to understand the origin of the topographical variation in

T_2 relaxation time.

Similar to previous reports [61, 160], an extra high-T_2 lamina, possibly related to the high chondrocyte density observed at the same sites, was often observed in deep cartilage (II). As suggested by PLM, the chondrocytes may force the course of collagen fibrils from a radial arrangement more towards the magic angle with corresponding higher T_2 values. Also, provided that the cells occupy a large volume, intracellular fluid which has only a few relaxation pathways could contribute to the high T_2 values found in deep tissue.

In normal and PG-depleted tissue, PG-sensitive MR parameters $T_{1\mathrm{Gd}}$ and [Gd-DTPA] correlated with the spatial GAG content of tissue, semiquantitatively assessed by DD. In deep cartilage, however, this correlation was impaired, for which several reasons can be suggested. First, Gd-DTPA relaxivity may vary with tissue depth. Interestingly, in the light of previous [145] and current findings (III) on the positive relaxivity-macromolecule content dependence, accounting for this effect would lead to a further overestimation of PG content by the MR technique, opposite to the findings of the present study. Yet, relaxivity of Gd-DTPA in some tissues has been reported to be even smaller than in saline, possibly due to compartmentalization of tissue water [138, 165]. Also, the present relaxivity measurements were conducted in phantoms with disordered proteins as opposed to cartilage with highly arranged proteins, and thus do not necessarily reflect the situation in cartilage. In cartilage, macromolecule loss through the depletion of collagen could alter the relaxivity of tissue, and thus weaken the specificity of the technique. Second, the penetration of Gd-DTPA may not be solely controlled by FCD, but could be affected by permeability and high solid content of tissue. Third, the pH of normal and diseased cartilage may vary with tissue depth, and possibly could affect the charge of Gd-DTPA and consequently its distribution. Thus, there are still several open questions that demand for further investigation.

The *in vivo* dGEMRIC measurements with asymptomatic volunteers mostly reproduced the same increasing pattern of T_1 relaxation time as observed *in vitro*. The *in vivo* finding can be attributed to the increasing PG concentration from surface to deep tissue known to exist in normal human tissue [101, 81]. Nonetheless, this should be confirmed with cadaver studies. The difference in $T_{1\mathrm{Gd}}$ values between medial and lateral compartments of the femur are in line with a previous dGEMRIC study [149]. The comparison of $T_{1\mathrm{Gd}}$ values between patella and femur, however, was not in agreement with an investigation that reported a higher PG content in the femur than in the patella [51]. The apparent mismatch may result from a regional variability in the uptake and wash-out of contrast agent [150] or a different effective equilibrating concentration for different articular surfaces thus affecting the measured T_1 values. Therefore, it would appear that a quantitative comparison within dGEMRIC experiments possibly can be performed only within a single articular surface. The *in vivo* study with ACT patients revealed relatively high T_1 values of

repaired tissue as compared to the control site, suggesting that PG replenishment had taken place after ACT surgery. This agrees with a recent dGEMRIC study on ACT grafts [55]. A higher imaging resolution would likely provide more information on normal and engineered tissue. Due to the limited number of cases studied, these preliminary findings have to be supplemented with more data.

9.2 Quantitative MRI and mechanical properties of cartilage

In study I, the T_2 response was accompanied by a parallel decrease in Young's modulus. Mechanical properties of the tissue were altered also after PG cleavage by chondroitinase ABC, but this was not detected by the T_2 measurements. Thus, T_2 does not appear to be an unambiguous indicator of cartilage stiffness.

Study IV involved a more systematic approach for investigating the usefulness of MR parameters in predicting the mechanical properties of cartilage. Both collagen- and PG-sensitive MR parameters showed moderate to high correlations with equilibrium moduli. Although a single MR parameter correlated with various mechanical parameters in normal tissue, the information from studies I and III point to the fact that at least both collagen- and PG-sensitive MR parameters are required for indirect mechanical characterization of tissue. The results are parallel to those reported in two preliminary studies correlating quantitative MRI and cartilage biomechanics [133, 156].

In the *in vivo* study with ACT patients, arthroscopic stiffness measurements showed that the repair tissue had not reached a mechanical integrity comparable to normal tissue, whereas dGEMRIC pointed to GAG replenishment. The elastic stiffness in a short-term compression is sensitive to the collagen structure of the tissue (see Section 4.3), and it is likely that the engineered tissue still lacks the three dimensional collagen architecture necessary for the normal mechanical integrity of cartilage. This is in line with a previous *in vitro* study that revealed the insensitivity of arthroscopic stiffness measurements to the PG component of cartilage [97]. Presumably, T_2 relaxation time mapping could have revealed if this was the case. It should also be noted that should the relaxivity of normal and engineered tissue be different, this would have an effect on the PG-quantizations from T_1 maps. Thus, further *ex vivo* and *in vivo* work is necessary.

Chapter X

Summary and conclusions

Quantitative MRI of articular cartilage holds great potential for the noninvasive diagnostics of cartilage-related diseases, particularly by enabling the assessment of relaxation processes related to the different macromolecular constituents of the tissue. Future developments in MR technology and instrumentation will further increase the feasibility of quantitative MRI techniques.

The present study investigated two potential quantitative MRI techniques, mainly applied at a high field strength allowing superior resolution. Specifically, the relationship of ^{1}H NMR relaxation characteristics in articular cartilage with the structural and compositional environment and functional properties was studied and correlated with a variety of reference techniques. Preliminary *in vivo* results were also presented. The following conclusions can be drawn:

- T_2 relaxation time is sensitive to the integrity of the collagen network;
- T_2 anisotropy in cartilage can be related to spatial variations in the three-dimensional collagen architecture;
- Gd-DTPA -enhanced T_1 imaging can reveal spatial changes in the PG content of tissue in normal and enzymatically degraded tissue, although some overestimation of deep cartilage PGs may occur;
- T_2 relaxation time and Gd-DTPA -enhanced T_1 imaging are probes for assessing the integrity of tissue macromolecules and can be used to estimate the mechanical competence of cartilage *in vitro*;
- delayed Gd-DTPA -enhanced MR imaging of cartilage is a promising technique *in vivo* for revealing (*i*) the spatial variation of the PG concentration and (*ii*) the replenishment of PGs in surgically treated tissue. The latter, however, may not be indicative of complete mechanical recovery of tissue.

REFERENCES

[1] Akella SV, Regatte RR, Gougoutas AJ, Borthakur A, Shapiro EM, Kneeland JB, Leigh JS, Reddy R. Proteoglycan-induced changes in $T_{1\rho}$-relaxation of articular cartilage at 4T. Magn Reson Med 46: 419–423, 2001.

[2] Akizuki S, Mow VC, Muller F, Pita JC, Howell DS, Manicourt DH. Tensile properties of human knee joint cartilage: I. Influence of ionic conditions, weight bearing, and fibrillation on the tensile modulus. J Orthop Res 4: 379–392, 1986.

[3] Allen RG, Burstein D, Gray ML. Monitoring glycosaminoglycan replenishment in cartilage explants with gadolinium-enhanced magnetic resonance imaging. J Orthop Res 17: 430–436, 1999.

[4] Alparslan L, Winalski C, Boutin R, Minas T. Postoperative magnetic resonance imaging of articular cartilage repair. Semin Musculoskelet Radiol 5: 345–363, 2001.

[5] Andrew E, Bradbury A, Eades R. Removal of dipolar broadening of nuclear magnetic resonance spectra of solids by specimen rotation. Nature 27: 1802–1803, 1959.

[6] Armstrong CG, Mow VC. Variations in the intrinsic mechanical properties of human articular cartilage with age, degeneration, and water content. J Bone Joint Surg Am 64: 88–94, 1982.

[7] Arokoski JP, Hyttinen MM, Helminen HJ, Jurvelin JS. Biomechanical and structural characteristics of canine femoral and tibial cartilage. J Biomed Mater Res 48: 99–107, 1999.

[8] Arokoski JP, Hyttinen MM, Lapveteläinen T, Takács P, Kosztáczky B, Módis L, Kovanen V, Helminen H. Decreased birefringence of the superficial zone collagen network in the canine knee (stifle) articular cartilage after long distance running training, detected by quantitative polarised light microscopy. Ann Rheum Dis 55: 253–264, 1996.

[9] Athanasiou KA, Agarwal A, Dzida FJ. Comparative study of the intrinsic mechanical properties of the human acetabular and femoral head cartilage. J Orthop Res 12: 340–349, 1994.

[10] Athanasiou KA, Niederauer GG, Schenck R. C. J. Biomechanical topography of human ankle cartilage. Ann Biomed Eng 23: 697–704, 1995.

[11] Athanasiou KA, Rosenwasser MP, Buckwalter JA, Malinin TI, Mow VC. Interspecies comparisons of in situ intrinsic mechanical properties of distal femoral car-

tilage. J Orthop Res 9: 330–340, 1991.

[12] Bacic G, Liu KJ, Goda F, Hoopes PJ, Rosen GM, Swartz HM. MRI contrast enhanced study of cartilage proteoglycan degradation in the rabbit knee. Magn Reson Med 37: 764–768, 1997.

[13] Bader DL, Kempson GE. The short-term compressive properties of adult human articular cartilage. Biomed Mater Eng 4: 245–256, 1994.

[14] Bank RA, Soudry M, Maroudas A, Mizrahi J, TeKoppele JM. The increased swelling and instantaneous deformation of osteoarthritic cartilage is highly correlated with collagen degradation. Arthritis Rheum 43: 2202–2210, 2000.

[15] Bashir A, Gray ML, Boutin RD, Burstein D. Glycosaminoglycan in articular cartilage: *in vivo* assessment with delayed Gd(DTPA)(2-)-enhanced MR imaging. Radiology 205: 551–558, 1997.

[16] Bashir A, Gray ML, Burstein D. Gd-DTPA^{2-} as a measure of cartilage degradation. Magn Reson Med 36: 665–673, 1996.

[17] Bashir A, Gray ML, Hartke J, Burstein D. Nondestructive imaging of human cartilage glycosaminoglycan concentration by MRI. Magn Reson Med 41: 857–865, 1999.

[18] Bennett HS. Methods applicable to the study of both fresh and fixed materials. The microscopical investigation of biological materials with polarized light. J McClung, ed., McClung's handbook of microscopical technique, pp. 591–677. Paul B Hoeber, New York, 1950.

[19] Benninghoff A. Form und Bau der Gelenkknorpel in ihren Beziehungen zur Function. Erste Mitteilung: die modellierenden und formerhaltenden Faktoren des Knorpelreliefs. Z Anat 76: 43–63, 1925.

[20] Berendsen H. Nuclear magnetic resonance study of collagen hydration. J Chem Phys 36: 3297–3305, 1962.

[21] Bloembergen N. Proton relaxation times in paramagnetic solutions. J Chem Phys 27: 572–573, 1957.

[22] Brocklehurst R, Bayliss MT, Maroudas A, Coysh HL, Freeman MA, Revell PA, Ali SY. The composition of normal and osteoarthritic articular cartilage from human knee joints. With special reference to unicompartmental replacement and osteotomy of the knee. J Bone Joint Surg Am 66: 95–106, 1984.

[23] Broom ND, Poole CA. Articular cartilage collagen and proteoglycans. Their functional interdependency. Arthritis Rheum 26: 1111–1119, 1983.

[24] Bryant RG. The dynamics of water-protein interactions. Annu Rev Biophys Biomol Struct 25: 29–53, 1996.

[25] Buckwalter J, Mankin H. Articular Cartilage, Part II: Degeneration and osteoarthritis, repair, regeneration, and transplantation. J Bone Joint Surg Am 79: 612–632, 1997.

[26] Burstein D, Bashir A, Gray ML. MRI techniques in early stages of cartilage disease. Invest Radiol 35: 622–638, 2000.

[27] Burstein D, Gray ML, Hartman AL, Gipe R, Foy BD. Diffusion of small solutes in cartilage as measured by nuclear magnetic resonance (NMR) spectroscopy and

imaging. J Orthop Res 11: 465–478, 1993.

[28] Burstein D, Velyvis J, Scott KT, Stock KW, Kim YJ, Jaramillo D, Boutin RD, Gray ML. Protocol issues for delayed Gd(DTPA)(2-)-enhanced MRI (dGEMRIC) for clinical evaluation of articular cartilage. Magn Reson Med 45: 36–41, 2001.

[29] Buschmann MD, Soulhat J, Shirazi-Adl A, Jurvelin JS, Hunziker EB. Confined compression of articular cartilage: linearity in ramp and sinusoidal tests and the importance of interdigitation and incomplete confinement. J Biomech 31: 171–178, 1998.

[30] Callahan P. Principles of nuclear magnetic resonance microscopy. Oxford University Press, New York, 1991.

[31] Chandnani VP, Ho C, Chu P, Trudell D, Resnick D. Knee hyaline cartilage evaluated with MR imaging: a cadaveric study involving multiple imaging sequences and intraarticular injection of gadolinium and saline solution. Radiology 178: 557–561, 1991.

[32] Cohen B, Lai WM, Mow VC. A transversely isotropic biphasic model for unconfined compression of growth plate and chondroepiphysis. J Biomech Eng 120: 491–496, 1998.

[33] Collins DH, McElliot TF. Sulphate ($^{35}SO_4$) uptake by chondrocytes in relation to histological changes in osteoarthritic human articular cartilage. Ann Rheum Dis 19: 318–330, 1960.

[34] Cova M, Toffanin R, Frezza F, Pozzi-Mucelli M, Mlynárik V, Pozzi-Mucelli RS, Vittur F, Dalla-Palma L. Magnetic resonance imaging of articular cartilage: ex vivo study on normal cartilage correlated with magnetic resonance microscopy. Eur Radiol 8: 1130–1136, 1998.

[35] Cowan B. Nuclear magnetic resonance and relaxation. University Press, Cambridge, 1997.

[36] Dardzinski BJ, Mosher TJ, Li S, Van Slyke MA, Smith MB. Spatial variation of T_2 in human articular cartilage. Radiology 205: 546–550, 1997.

[37] Donahue KM, Burstein D, Manning WJ, Gray ML. Studies of Gd-DTPA relaxivity and proton exchange rates in tissue. Magn Reson Med 32: 66–76, 1994.

[38] Duvvuri U, Charagundla SR, Kudchodkar SB, Kaufman JH, Kneeland JB, Rizi R, Leigh JS, Reddy R. Human knee: *in vivo* $T_{1\rho}$-weighted MR imaging at 1.5T - preliminary experience. Radiology 220: 822–826., 2001.

[39] Duvvuri U, Goldberg A, Kranz J, Hoang L, Reddy R, Wehrli F, Wand A, Englander S, Leigh J. Water magnetic relaxation dispersion in biological systems: The contribution of proton exchange and implications for the noninvasive detection of cartilage degradation. Proc Natl Acad Sci 98: 12479–12484, 2001.

[40] Duvvuri U, Reddy R, Patel SD, Kaufman JH, Kneeland JB, Leigh JS. $T_{1\rho}$-relaxation in articular cartilage: effects of enzymatic degradation. Magn Reson Med 38: 863–867, 1997.

[41] Eckstein F, Reiser M, Englmeier KH, Putz R. *In vivo* morphometry and functional analysis of human articular cartilage with quantitative magnetic resonance imaging–from image to data, from data to theory. Anat Embryol 203: 147–173, 2001.

[42] Eisenberg SR, Grodzinsky AJ. Swelling of articular cartilage and other connective tissues: electromechanochemical forces. J Orthop Res 3: 148–159, 1985.

[43] Erickson SJ, Waldschmidt JG, Czervionke LF, Prost RW. Hyaline cartilage: truncation artifact as a cause of trilaminar appearance with fat-suppressed three-dimensional spoiled gradient- recalled sequences. Radiology 201: 260–264, 1996.

[44] Eyre DR, Wu JJ. Collagen structure and cartilage matrix integrity. J Rheumatol Suppl 43: 82–85, 1995.

[45] Fragonas E, Mlynárik V, Jellús V, Micali F, Piras A, Toffanin R, Rizzo R, Vittur F. Correlation between biochemical composition and magnetic resonance appearance of articular cartilage. Osteoarthritis Cartilage 6: 24–32, 1998.

[46] Frank EH, Grodzinsky AJ. Cartilage electromechanics–I. Electrokinetic transduction and the effects of electrolyte pH and ionic strength. J Biomech 20: 615–627, 1987.

[47] Frank EH, Grodzinsky AJ. Cartilage electromechanics–II. A continuum model of cartilage electrokinetics and correlation with experiments. J Biomech 20: 629–639, 1987.

[48] Frank LR, Brossmann J, Buxton RB, Resnick D. MR imaging truncation artifacts can create a false laminar appearance in cartilage. Am J Roentgenol 168: 547–554, 1997.

[49] Frank LR, Wong EC, Luh WM, Ahn JM, Resnick D. Articular cartilage in the knee: mapping of the physiologic parameters at MR imaging with a local gradient coil–preliminary results. Radiology 210: 241–246, 1999.

[50] Freeman DM, Bergman G, Glover G. Short TE MR microscopy: accurate measurement and zonal differentiation of normal hyaline cartilage. Magn Reson Med 38: 72–81, 1997.

[51] Froimson MI, Ratcliffe A, Gardner TR, Mow VC. Differences in patellofemoral joint cartilage material properties and their significance to the etiology of cartilage surface fibrillation. Osteoarthritis Cartilage 5: 377–386, 1997.

[52] Fullerton G. Physiologic basis of magnetic relaxation. D Stark, W Bradley, eds., Magnetic resonance imaging, pp. 36–54. Bradley, Baltimore, 1992.

[53] Fullerton GD, Cameron IL, Ord VA. Orientation of tendons in the magnetic field and its effect on T_2 relaxation times. Radiology 155: 433–435, 1985.

[54] Garwood M, Ke Y. Symmetric pulses to induce arbitrary flip angles with compensation for RF inhomogeneity and resonance offsets. J Magn Reson 94: 511–525, 1991.

[55] Gillis A, Bashir A, McKeon B, Scheller A, Gray M, Burstein D. Magnetic resonance imaging of relative glycosaminoglycan distribution in patients with autologous chondrocyte transplants. Invest Radiol 36: 743–748, 2001.

[56] Gillis A, Gray M, Burstein D. Relaxivity of gadolinium agents in cartilage at 2T: Effects on dGEMRIC imaging. Proc Intl Soc Mag Reson Med 9: 34, 2001.

[57] Gomez S, Toffanin R, Bernstorff S, Romanello M, Amenitsch H, Rappolt M, Rizzo R, Vittur F. Collagen fibrils are differently organized in weight-bearing and not-weight-bearing regions of pig articular cartilage. J Exp Zool 287: 346–352, 2000.

[58] Goodwin DW, Dunn JF. High-resolution magnetic resonance imaging of articular cartilage: correlation with histology and pathology. Top Magn Reson Imaging 9: 337–347, 1998.

[59] Goodwin DW, Zhu H, Dunn JF. *In vitro* MR imaging of hyaline cartilage: correlation with scanning electron microscopy. Am J Roentgenol 174: 405–409, 2000.

[60] Gray ML, Burstein D, Lesperance LM, Gehrke L. Magnetization transfer in cartilage and its constituent macromolecules. Magn Reson Med 34: 319–325, 1995.

[61] Gründer W, Kanowski M, Wagner M, Werner A. Visualization of pressure distribution within loaded joint cartilage by application of angle-sensitive NMR microscopy. Magn Reson Med 43: 884–891, 2000.

[62] Gründer W, Wagner M, Werner A. MR-microscopic visualization of anisotropic internal cartilage structures using the magic angle technique. Magn Reson Med 39: 376–382, 1998.

[63] Grodzinsky AJ. Electromechanical and physicochemical properties of connective tissue. Crit Rev Biomed Eng 9: 133–199, 1983.

[64] Haacke E, Brown R, Thompson M, Venkatesan R. Magnetic resonance imaging: physical principles and sequence design. John Wiley Sons, New York, 1999.

[65] Hardingham T. Proteoglycans and glycosaminoglycans. M Seibel, S Robins, J Bilezikian, eds., Dynamics of bone and cartilage metabolism, pp. 3–29. Academic Press, San Diego, 1999.

[66] Hayes WC, Bodine AJ. Flow-independent viscoelastic properties of articular cartilage matrix. J Biomech 11: 407–419, 1978.

[67] Hayes WC, Keer LM, Herrmann G, Mockros LF. A mathematical analysis for indentation tests of articular cartilage. J Biomech 5: 541–551, 1972.

[68] Henkelman RM, Stanisz GJ, Graham SJ. Magnetization transfer in MRI: a review. NMR Biomed 14: 57–64, 2001.

[69] Henkelman RM, Stanisz GJ, Kim JK, Bronskill MJ. Anisotropy of NMR properties of tissues. Magn Reson Med 32: 592–601, 1994.

[70] Hudelmaier M, Glaser C, Hohe J, Englmeier KH, Reiser M, Putz R, Eckstein F. Age-related changes in the morphology and deformational behavior of knee joint cartilage. Arthritis Rheum 44: 2556–2561, 2001.

[71] Jurvelin JS, Buschmann MD, Hunziker EB. Mechanical anisotropy of human knee articular cartilage in compression. Transact Orthop Res Soc 21: 7, 1996.

[72] Jurvelin JS, Buschmann MD, Hunziker EB. Optical and mechanical determination of Poisson's ratio of adult bovine humeral articular cartilage. J Biomech 30: 235–241, 1997.

[73] Jurvelin JS, Räsänen T, Kolmonen P, Lyyra T. Comparison of optical, needle probe and ultrasonic techniques for the measurement of articular cartilage thickness. J Biomech 28: 231–235, 1995.

[74] Kaufman JH, Regatte RR, Bolinger L, Kneeland JB, Reddy R, Leigh JS. A novel approach to observing articular cartilage deformation *in vitro* via magnetic resonance imaging. J Magn Reson Imaging 9: 653–662, 1999.

[75] Kempson GE, Muir H, Swanson SAV, Freeman MAR. Correlations between stiffness

and the chemical constituents of cartilage on the human femoral head. Biochim Biophys Acta 215: 70–77, 1970.

[76] Kim DJ, Suh JS, Jeong EK, Shin KH, Yang WI. Correlation of laminated MR appearance of articular cartilage with histology, ascertained by artificial landmarks on the cartilage. J Magn Reson Imaging 10: 57–64, 1999.

[77] Kim DK, Ceckler TL, Hascall VC, Calabro A, Balaban RS. Analysis of water-macromolecule proton magnetization transfer in articular cartilage. Magn Reson Med 29: 211–215, 1993.

[78] Király K, Hyttinen MM, Lapveteläinen T, Elo M, Kiviranta I, Dobai J, Módis L, Helminen HJ, Arokoski JP. Specimen preparation and quantification of collagen birefringence in unstained sections of articular cartilage using image analysis and polarizing light microscopy. Histochem J 29: 317–327, 1997.

[79] Király K, Lammi M, Arokoski J, Lapveteläinen T, Tammi M, Helminen H, Kiviranta I. Safranin O reduces loss of glycosaminoglycans from bovine articular cartilage during histological specimen preparation. Histochem J 28: 99–107, 1996.

[80] Király K, Lapveteläinen T, Arokoski J, Törrönen K, Módis L, Kiviranta I, Helminen HJ. Application of selected cationic dyes for the semiquantitative estimation of glycosaminoglycans in histological sections of articular cartilage by microspectrophotometry. Histochem J 28: 577–590, 1996.

[81] Kiviranta I, Jurvelin J, Tammi M, Säämänen AM, Helminen HJ. Microspectrophotometric quantitation of glycosaminoglycans in articular cartilage sections stained with Safranin O. Histochemistry 82: 249–255, 1985.

[82] Koenig S, Brown III R. Relaxometry and the source of contrast in MRI. R Gillies, ed., NMR in physiology and biomedicine, pp. 57–73. Academic Press, Inc., San Diego, 1994.

[83] Korhonen R, Wong M, Arokoski J, Lindgren R, Helminen H, Hunziker E, Jurvelin J. Importance of the superficial tissue layer for the indentation stiffness of articular cartilage. Med Eng Phys 24: 99–108, 2002.

[84] Kusaka Y, Gründer W, Rumpel H, Dannhauer KH, Gersonde K. MR microimaging of articular cartilage and contrast enhancement by manganese ions. Magn Reson Med 24: 137–148, 1992.

[85] Lai WM, Hou JS, Mow VC. A triphasic theory for the swelling and deformation behaviors of articular cartilage. J Biomech Eng 113: 245–258, 1991.

[86] Lattanzio PJ, Marshall KW, Damyanovich AZ, Peemoeller H. Macromolecule and water magnetization exchange modeling in articular cartilage. Magn Reson Med 44: 840–851, 2000.

[87] Lauffer RB. Paramagnetic metal complexes as water proton relaxation agents for NMR imaging: Theory and design. Chem Rev 87: 901–927, 1987.

[88] Lee RC, Frank EH, Grodzinsky AJ, Roylance DK. Oscillatory compressional behavior of articular cartilage and its associated electromechanical properties. J Biomech Eng 103: 280–292, 1981.

[89] Lehner KB, Rechl HP, Gmeinwieser JK, Heuck AF, Lukas HP, Kohl HP. Structure, function, and degeneration of bovine hyaline cartilage: assessment with MR imaging

in vitro. Radiology 170: 495–499, 1989.

[90] Lemperg RK, Larsson SE, Hjertquist SO. Distribution of water and glycosaminoglycans in different layers of cattle articular cartilage. Isr J Med Sci 7: 419–421, 1971.

[91] Lesperance LM, Gray ML, Burstein D. Determination of fixed charge density in cartilage using nuclear magnetic resonance. J Orthop Res 10: 1–13, 1992.

[92] Lewitt M, Park B. Water: now you see it, now you don't. Structure 15: 223–226, 1993.

[93] Li LP, Buschmann MD, Shirazi-Adl A. A fibril reinforced nonhomogeneous poroelastic model for articular cartilage: inhomogeneous response in unconfined compression. J Biomech 33: 1533–1541, 2000.

[94] Lüsse S, Claassen H, Gehrke T, Hassenpflug J, Schünke M, Heller M, Glüer CC. Evaluation of water content by spatially resolved transverse relaxation times of human articular cartilage. Magnetic Resonance Imaging 18: 423–430, 2000.

[95] Lüsse S, Knauss R, Werner A, Gründer W, Arnold K. Action of compression and cations on the proton and deuterium relaxation in cartilage. Magn Reson Med 33: 483–489, 1995.

[96] Luna L. Manual of histologic staining methods of the armed forces institute of pathology. McGraw-Hill, New York, 1968.

[97] Lyyra T, Arokoski JP, Oksala N, Vihko A, Hyttinen M, Jurvelin JS, Kiviranta I. Experimental validation of arthroscopic cartilage stiffness measurement using enzymatically degraded cartilage samples. Phys Med Biol 44: 525–535, 1999.

[98] Lyyra T, Jurvelin J, Pitkänen P, Väätäinen U, Kiviranta I. Indentation instrument for the measurement of cartilage stiffness under arthroscopic control. Med Eng Phys 17: 395–399, 1995.

[99] Mankin HJ, Thrasher AZ. Water content and binding in normal and osteoarthritic human cartilage. J Bone Joint Surg Am 57: 76–80, 1975.

[100] Maroudas A. Physico-chemical properties of articular cartilage. M Freeman, ed., Adult articular cartilage, pp. 131–170. Pitman Medical, Kent, 1973.

[101] Maroudas A, Bayliss MT, Venn MF. Further studies on the composition of human femoral head cartilage. Ann Rheum Dis 39: 514–523, 1980.

[102] Maroudas A, Bullough P, Swanson SA, Freeman MA. The permeability of articular cartilage. J Bone Joint Surg Br 50: 166–177, 1968.

[103] Maroudas A, Schneiderman R. "Free" and "exchangeable" or "trapped" and "non-exchangeable" water in cartilage. J Orthop Res 5: 133–138, 1987.

[104] Maroudas A, Venn M. Chemical composition and swelling of normal and osteoarthrotic femoral head cartilage. II. Swelling. Ann Rheum Dis 36: 399–406, 1977.

[105] Maroudas AI. Balance between swelling pressure and collagen tension in normal and degenerate cartilage. Nature 260: 808–809, 1976.

[106] McCauley T, Recht M, Disler D. Clinical imaging of articular cartilage in the knee. Semin Musculoskelet Radiol 5, 2001.

[107] Meachim G, Stockwell R. The matrix. M Freeman, ed., Adult articular cartilage,

pp. 1–50. Pitman Medical, Kent, 1973.

[108] Migchelsen C, Berendsen H. Proton exchange and molecular orientation of water in hydrated collagen fibers. An NMR study of H_20 and D_20. J Chem Phys 59: 296–305, 1973.

[109] Mizrahi J, Maroudas A, Lanir Y, Ziv I, Webber TJ. The "instantaneous" deformation of cartilage: effects of collagen fiber orientation and osmotic stress. Biorheology 23: 311–330, 1986.

[110] Mlynárik V, Degrassi A, Toffanin R, Vittur F, Cova M, Pozzi-Mucelli RS. Investigation of laminar appearance of articular cartilage by means of magnetic resonance microscopy. Magn Reson Imaging 14: 435–442, 1996.

[111] Mlynárik V, Trattnig S. Physicochemical properties of normal articular cartilage and its MR appearance. Invest Radiol 35: 589–594, 2000.

[112] Mlynárik V, Trattnig S, Huber M, Zembsch A, Imhof H. The role of relaxation times in monitoring proteoglycan depletion in articular cartilage. J Magn Reson Imaging 10: 497–502, 1999.

[113] Modl JM, Sether LA, Haughton VM, Kneeland JB. Articular cartilage: correlation of histologic zones with signal intensity at MR imaging. Radiology 181: 853–855, 1991.

[114] Mosher TJ, Dardzinski BJ, Smith MB. Human articular cartilage: influence of aging and early symptomatic degeneration on the spatial variation of T_2 - preliminary findings at 3T. Radiology 214: 259–266, 2000.

[115] Mosher TJ, Smith H, Dardzinski BJ, Schmithorst VJ, Smith MB. MR imaging and T_2 mapping of femoral cartilage: *in vivo* determination of the magic angle effect. Am J Roentgenol 177: 665–669, 2001.

[116] Mow VC, Kuei SC, Lai WM, Armstrong CG. Biphasic creep and stress relaxation of articular cartilage in compression: Theory and experiments. J Biomech Eng 102: 73–84, 1980.

[117] Mow VC, Ratcliffe A, Poole AR. Cartilage and diarthrodial joints as paradigms for hierarchical materials and structures. Biomaterials 13: 67–97, 1992.

[118] Mow VC, Zhu W, Ratcliffe A. Structure and function of articular cartilage and meniscus. VC Mow, WC Hayes, eds., Basic orthopaedic biomechanics, pp. 143–198. Raven Press, Ltd, New York, 1991.

[119] Muir H. The chondrocyte, architect of cartilage. Biomechanics, structure, function and molecular biology of cartilage matrix macromolecules. Bioessays 17: 1039–1048, 1995.

[120] Navon G, Shinar H, Eliav U, Seo Y. Multiquantum filters and order in tissues. NMR Biomed 14: 112–132., 2001.

[121] Newman AP. Articular cartilage repair. American Journal of Sports Medicine 26: 309–324, 1998.

[122] Ogawa S, Menon R, Tank D, Kim SG, Merkle H, Ellerman J, Ugurbil K. Functional brain mapping by blood oxygenation level dependent contrast magnetic resonance imaging. Biophys J 64: 803–812, 1993.

[123] Parsons JR, Black J. The viscoelastic shear behavior of normal rabbit articular

cartilage. J Biomech 10: 21–29, 1977.

[124] Paul PK, Jasani MK, Sebok D, Rakhit A, Dunton AW, Douglas FL. Variation in MR signal intensity across normal human knee cartilage. J Magn Reson Imaging 3: 569–574, 1993.

[125] Peto S, Gillis P. Fiber-to-field angle dependence of proton nuclear magnetic relaxation in collagen. Magn Reson Imaging 8: 705–712, 1990.

[126] Pottenger LA, Lyon NB, Hecht JD, Neustadt PM, Robinson RA. Influence of cartilage particle size and proteoglycan aggregation on immobilization of proteoglycans. J Biol Chem 257: 11479–11485, 1982.

[127] Quinn TM, Dierickx P, Grodzinsky AJ. Glycosaminoglycan network geometry may contribute to anisotropic hydraulic permeability in cartilage under compression. J Biomech 34: 1483–1490, 2001.

[128] Quinn TM, Morel V, Meister JJ. Static compression of articular cartilage can reduce solute diffusivity and partitioning: implications for the chondrocyte biological response. J Biomech 34: 1463–1469, 2001.

[129] Radin EL, Paul IL, Tolkoff MJ. Subchondral bone changes in patients with early degenerative joint disease. Arthritis Rheum 13: 400–405, 1970.

[130] Reddy R, Insko EK, Noyszewski EA, Dandora R, Kneeland JB, Leigh JS. Sodium MRI of human articular cartilage *in vivo*. Magn Reson Med 39: 697–701, 1998.

[131] Rubenstein JD, Kim JK, Henkelman RM. Effects of compression and recovery on bovine articular cartilage: appearance on MR images. Radiology 201: 843–850, 1996.

[132] Rubenstein JD, Kim JK, Morova-Protzner I, Stanchev PL, Henkelman RM. Effects of collagen orientation on MR imaging characteristics of bovine articular cartilage. Radiology 188: 219–226, 1993.

[133] Samosky J, Burstein D, Martin S, Grimson E, Gray M. Spatially-localized GAG mapping with dGEMRIC predicts the compressive load response of the articular surface to in situ indentation testing. Transact Orthop Res Soc 27: 403, 2002.

[134] Schmidt MB, Mow VC, Chun LE, Eyre DR. Effects of proteoglycan extraction on the tensile behavior of articular cartilage. J Orthop Res 8: 353–363, 1990.

[135] Seo GS, Aoki J, Moriya H, Karakida O, Sone S, Hidaka H, Katsuyama T. Hyaline cartilage: *in vivo* and *in vitro* assessment with magnetization transfer imaging. Radiology 201: 525–530, 1996.

[136] Shapiro EM, Borthakur A, Dandora R, Kriss A, Leigh JS, Reddy R. Sodium visibility and quantitation in intact bovine articular cartilage using high field ^{2}3Na MRI and MRS. J Magn Reson 142: 24–31, 2000.

[137] Shapiro EM, Borthakur A, Kaufman JH, Leigh JS, Reddy R. Water distribution patterns inside bovine articular cartilage as visualized by ^{1}H magnetic resonance imaging. Osteoarthritis Cartilage 9: 533–538, 2001.

[138] Shuter B, Wang SC, Roche J, Briggs G, Pope JM. Relaxivity of Gd-EOB-DTPA in the normal and biliary obstructed guinea pig. J Magn Reson Imaging 8: 853–861, 1998.

[139] Simon WH. Scale effects in animal joints. I. Articular cartilage thickness and com-

pressive stress. Arthritis Rheum 13: 244–256, 1970.

[140] Smith HE, Mosher TJ, Dardzinski BJ, Collins BG, Collins CM, Yang QX, Schmithorst VJ, Smith MB. Spatial variation in cartilage T_2 of the knee. J Magn Reson Imaging 14: 50–55, 2001.

[141] Solomon I. Relaxation processes in a system of two spins. Physical Review 99: 559–565, 1955.

[142] Soulhat J, Buschmann MD, Shirazi-Adl A. A fibril-network-reinforced biphasic model of cartilage in unconfined compression. J Biomech Eng 121: 340–347, 1999.

[143] Spilker RL, Suh JK, Mow VC. A finite element analysis of the indentation stress-relaxation response of linear biphasic articular cartilage. J Biomech Eng 114: 191–201, 1992.

[144] Stammberger T, Eckstein F, Englmeier KH, Reiser M. Determination of 3D cartilage thickness data from MR imaging: computational method and reproducibility in the living. Magn Reson Med 41: 529–536., 1999.

[145] Stanisz GJ, Henkelman RM. Gd-DTPA relaxivity depends on macromolecular content. Magn Reson Med 44: 665–667, 2000.

[146] Stockwell R, Meachim G. The chondrocytes. M Freeman, ed., Adult articular cartilage, pp. 51–99. Pitman Medical, Kent, 1973.

[147] Studer D, Chiquet M, Hunziker EB. Evidence for a distinct water-rich layer surrounding collagen fibrils in articular cartilage extracellular matrix. J Struct Biol 117: 81–85, 1996.

[148] Sun Y, Luo Z, An K. Mechanical properties of single type II collagen molecule. Transact Orthop Res Soc 27: 82, 2002.

[149] Tiderius CJ, Olsson LE, de Verdier H, Leander P, Ekberg O, Dahlberg L. Gd-DTPA(2-)-enhanced MRI of femoral knee cartilage: a dose-response study in healthy volunteers. Magn Reson Med 46: 1067–1071, 2001.

[150] Trattnig S, Mlynárik V, Breitenseher M, Huber M, Zembsch A, Rand T, Imhof H. MRI visualization of proteoglycan depletion in articular cartilage via intravenous administration of Gd-DTPA. Magn Reson Imaging 17: 577–583, 1999.

[151] Töyräs J, Rieppo J, Nieminen MT, Helminen HJ, Jurvelin JS. Characterization of enzymatically induced degradation of articular cartilage using high frequency ultrasound. Phys Med Biol 44: 2723–2733, 1999.

[152] Uhl M, Ihling C, Allmann KH, Laubenberger J, Tauer U, Adler CP, Langer M. Human articular cartilage: *in vitro* correlation of MRI and histologic findings. Eur Radiol 8: 1123–1129, 1998.

[153] Venn M, Maroudas A. Chemical composition and swelling of normal and osteoarthrotic femoral head cartilage. I. Chemical composition. Ann Rheum Dis 36: 121–129, 1977.

[154] von der Mark K. Structure, biosynthesis, and gene regulation of collagens in cartilage and bone. M Seibel, S Robins, J Bilezikian, eds., Dynamics of bone and cartilage metabolism, pp. 3–29. Academic Press, San Diego, 1999.

[155] Wachsmuth L, Juretschke HP, Raiss RX. Can magnetization transfer magnetic resonance imaging follow proteoglycan depletion in articular cartilage? Magma 5:

71–78, 1997.

[156] Wayne J, Kraft K, Shields K, Owen J, Yin C, Disler D. Correlation of function and MRI in cartilage. Transact Orthop Res Soc 27: 364, 2002.

[157] Winalski CS, Aliabadi P, Wright RJ, Shortkroff S, Sledge CB, Weissman BN. Enhancement of joint fluid with intravenously administered gadopentetate dimeglumine: technique, rationale, and implications. Radiology 187: 179–185, 1993.

[158] Wong M, Ponticiello M, Kovanen V, Jurvelin JS. Volumetric changes of articular cartilage during stress relaxation in unconfined compression. J Biomech 33: 1049–1054, 2000.

[159] Xia Y. Relaxation anisotropy in cartilage by NMR microscopy (μMRI) at 14-μm resolution. Magn Reson Med 39: 941–949, 1998.

[160] Xia Y. Heterogeneity of cartilage laminae in MR imaging. J Magn Reson Imaging 11: 686–693, 2000.

[161] Xia Y, Farquhar T, Burton-Wurster N, Lust G. Origin of cartilage laminae in MRI. J Magn Reson Imaging 7: 887–894, 1997.

[162] Xia Y, Farquhar T, Burton-Wurster N, Ray E, Jelinski LW. Diffusion and relaxation mapping of cartilage-bone plugs and excised disks using microscopic magnetic resonance imaging. Magn Reson Med 31: 273–282, 1994.

[163] Xia Y, Farquhar T, Burton-Wurster N, Vernier-Singer M, Lust G, Helinski L. Self-diffusion monitors degraded cartilage. Arch Biochem Biophys 323: 323–328, 1995.

[164] Xia Y, Moody JB, Burton-Wurster N, Lust G. Quantitative in situ correlation between microscopic MRI and polarized light microscopy studies of articular cartilage. Osteoarthritis Cartilage 9: 393–406, 2001.

[165] Xie D, Kennan R, Gore J. Measurements of the relaxivity of gadolinium chelates in tissues *in vivo*. Proc Intl Soc Mag Reson Med 9: 890, 2001.

[166] Yelin E, Callahan LF. The economic cost and social and psychological impact of musculoskeletal conditions. National Arthritis Data Work Groups. Arthritis Rheum 38: 1351–1362, 1995.